

# **Assessing forest yield and site suitability for *Eucalyptus grandis* x *E. urophylla* in coastal Zululand, South Africa, under climate change scenarios**

by

**Tiza Ignatius Mfuni**



Thesis presented in partial fulfilment of the requirements for the degree of **Master of Science in Forestry and Natural Resources Science**

at

**Stellenbosch University**

Department of Forestry and Wood Sciences, Faculty of AgriSciences

*Supervisor:* Professor David Michael Drew

*Co-supervisor:* Doctor Ilaria Germishuizen

April 2022

## Declaration

By submitting this thesis electronically, I declare that the entirety of the work contained therein is my own, original work, that I am the sole author thereof (save to the extent explicitly otherwise stated), that reproduction and publication thereof by Stellenbosch University will not infringe any third-party rights and that I have not previously in its entirety or in part submitted it for obtaining any qualification.

Date: April 2022

Copyright © 2022 Stellenbosch University  
All rights reserved

## Summary

This study aimed to project future mean annual temperature (MAT), mean annual precipitation (MAP), species site suitability, forest yield and the risk of the *Leptocybe invasa* pest for *Eucalyptus grandis* x *urophylla* (*E. g* x *u*) in coastal Zululand of South Africa, under two emission scenarios (Representative Concentration Pathway (RCP) 4.5 and 8.5), each for the intermediate term (2041 – 2060) and long term (2081 – 2100). The study utilized projected future climate variables from Global Circulation Models (GCMs) used in phase five of the coupled Model Intercomparison Project (CMIP5) for use in the R version of 3PG (Physiological Processes Predicting Growth) to simulate forest stand volume. The climate data was also combined with recorded presence of the *Leptocybe invasa* pest to develop an ecological niche model using the Maximum Entropy (Maxent) model and project the possible risk of the pests' infestation in the study site. Generally, projected future climates revealed increasing MATs amid reducing MAP over most of the study points in both RCP 4.5 and 8.5 as well as shifts in species site suitability for *E. g* x *u*. After validating and testing the r3PG model for use in coastal Zululand using field data, the r3PG runs across the future scenarios projected a pattern of reducing volume yield for *E. g* x *u*. A second species that was tested, *Pinus elliotii*, exhibited a relatively more severe trend of reducing yields from the current scenario through the future scenarios. These projected changes were observed amidst a reducing risk of *L. invasa* over the study grid points in both pathways by the end of the century.

Even though the data had some inaccuracies, acquired from third party sources, and based on assumptions from GCMs, this study shows how integrating projected climate information, processed-based growth models and pest risk models can improve the information available to South Africa's Forest industry. The integration of these data and models could contribute to the preparedness of the forest industry and inform policymaking towards mitigating uncertain climate futures.

This thesis is dedicated to my selfless parents, Mr. Norbert K. Mfuni and Mrs. Annie Nakawakwe Mfuni. I am because you have been.

## Acknowledgements

I wish to express my sincerest gratitude and appreciation to the following persons and institutions:

- My supervisors: Prof David Michael Drew for taking a chance on me from the PGDip to this level, for the patience, for the push, for the mentorship, for the direction and for extending my knowledge to plantation forestry. I am extremely privileged to have had the opportunity to learn from his genius. To Dr. Ilaria Germishuizen, I am honoured to have been in her presence. I am thankful for all the advanced spatial modelling techniques, all the data and hands-on approaches, and making time to respond to messages, commenting on drafts and travelling down from UKZN when needed. Grazie mille!
- Dr. Kim Martin, for helping with the R-scripts and pipeline which greatly reduced the manual interventions needed and cut the analysis time to more than half of what it would've been. I am additionally grateful for her being a decent competitor in coffee consumption.
- Mr. Oluwaseun Gakenou for assisting me with understanding the workings of 3PG, the nature of the sites on the ground and the workings of the university as a whole.
- Dr Leandra Moller, for always being there to sort out technical issues.
- Mondi and Sappi for providing funding for this research
- The entire EucXylo team for shorting my learning curve during our interactions about the project and life in general.
- My colleagues at the Center for International Forestry Research (CIFOR) especially Dr. Davison Gumbo, Mr. Kaala Moombe and Mrs. Alice Siamutondo for making my work-school balance a lot easier.
- My PhD advisor at the Pennsylvania State University, Dr. Bronwen Powell, for giving me time and encouraging me to complete this stage of my education while pursuing my PhD studies.
- The faculty, staff and students of the Department of Forest and Wood Sciences for creating a good work environment and feedback during presentations.
- My family and friends for the encouragement and support.

## Table of Contents

Declaration.....	i
Summary.....	iii
Acknowledgements.....	v
Table of Contents.....	vi
List of Figures.....	viii
List of Tables.....	ix
List of abbreviations and acronyms.....	x
Chapter 1 General overview.....	1
1.1 Introduction.....	1
Chapter 2 Literature review.....	3
2.1 Modelling future climate.....	3
2.1.1 Global scenario of GCMs.....	3
2.1.2 IPCC AR5.....	3
2.1.3 GHG concentrations in climate models.....	4
2.2 GCMs in Southern Africa.....	6
2.3 Downscaling of GCMs.....	7
2.3.1 Dynamic downscaling.....	7
2.3.2 Statistical downscaling.....	8
2.4 Downscaled GCMs in southern Africa.....	8
2.4.1 CORDEX.....	9
2.4.2 Conformal-Cubic Atmospheric Model (CCAM).....	10
2.5 A changing climate in southern Africa.....	10
2.5.1 Future temperature and rainfall in South Africa.....	11
2.5.2 Climate in the Zululand region.....	12
2.6 Forestry in the Zululand coastal plain.....	13
2.7 Physiological Processes Predicting Growth (3-PG) Forest Growth Model.....	14
2.7.1 Effect of atmospheric CO <sub>2</sub> concentration on tree growth and 3PG modelling.....	16
Chapter 3 Materials and methods.....	18
3.1 Study area.....	18
3.2 Climate for long term projection models.....	19
3.3 Soils.....	22
3.4 r3PG runs and parameter assumptions.....	23
3.4.1 r3PG model validation.....	25
3.4.2 Actual weather data for model testing.....	26
3.4.3 Soils data for model testing.....	27
3.4.4 Atmospheric CO <sub>2</sub> concentration.....	28
3.5 Future climate runs.....	28
3.6 Site suitability and species choices.....	29
3.7 <i>Leptocybe invasa</i> pest modelling.....	30
Chapter 4 Results.....	33
4.1 Climate.....	33

4.1.1	Temperature.....	33
4.1.2	Precipitation.....	36
4.2	Future shifts in site species suitability .....	38
4.3	Testing and validating of the r3PG model .....	40
4.3.1	r3PG modelling and increasing atmospheric CO <sub>2</sub> concentration .....	41
4.4	Volume yield .....	41
4.5	<i>Leptocybe invasa</i> occurrence and risk .....	45
Chapter 5	Discussion and conclusion .....	48
5.1	Global circulation models and climate projections.....	48
5.2	Shifts in site types.....	49
5.3	3PG as a tool for predicting volume in eucalypt stands.....	50
5.4	Future volume expectations using 3PG.....	50
5.5	Pest risk.....	52
6	Conclusion .....	53
References.....		55
ANNEX 1	Mean annual precipitation change for each point in RCP 4.5.....	65
ANNEX 2	Mean annual precipitation change for each point in RCP 4.5.....	66

## List of Figures

<b>Figure 2.1:</b> GCMs that participated in the CMIP5 experiment (Flato et al., 2013) .....	5
<b>Figure 2.2:</b> Representative concentration pathways (RCP) in the AR5 (IPCC, 2014b) .....	6
<b>Figure 2.3:</b> The structure of the 3-PG model according to Trotsiuk et al. (2020) .....	15
<b>Figure 3.1:</b> Location of the study area over coastal Zululand. The red circles represent the 5x5 km point grid for which future climate projections were obtained. ....	19
<b>Figure 3.2:</b> RCPs considered in this study and the scenarios along those RCPs (IPCC, 2014b) .....	21
<b>Figure 3.3</b> Sub-tropical (ST) site classes for commercial plantation species based on ranges of mean annual precipitation and meant annual temperature (Source: Modified from Smith et al., 2005).....	30
<b>Figure 4.1</b> Projected mean annual temperature change under RCP 4.5 at each 5x5 grid point. The blue plus sign (+) represents current temperature (1970 – 2000), the green circle (○) intermediate temperature (2041 – 2060), and the red triangle ( ) future temperature (2081 – 2100).....	33
<b>Figure 4.2</b> Projected mean annual temperature change under RCP 8.5 at each 5x5 grid point. The blue plus sign (+) represents current temperature (1970 – 2000), the green circle (○) intermediate temperature (2041 – 2060), and the red triangle ( ) future temperature.....	35
<b>Figure 4.3</b> Change in precipitation from the year 2000 to 2041 (left) and to 2081 (right) for RCP 4.5. The precipitation change is shown on a colour scale from red, representing the biggest loss, to navy blue representing a gain in precipitation.....	36
<b>Figure 4.4</b> Change in precipitation from the year 2000 to 2041 (left) and to 2081 (right) from the WorldClim data for RCP 8.5. The precipitation change is shown on a colour scale from red, representing the biggest loss, to navy blue representing a gain in precipitation.....	37
<b>Figure 4.5</b> The projected site classification shifts for the study region over projected precipitation for the respective scenario.....	39
<b>Figure 4.6:</b> Plot of r3PG modelled volume against field observed volume in the 18 test sites... 40	40
<b>Figure 4.7:</b> Modelled current and projected <i>Eucalyptus grandis x urophylla</i> stand volume at the end of a 7-year rotation on the 5x5 grid points. ....	43
<b>Figure 4.8:</b> Modelled current and projected <i>Pinus elliottii</i> stand volume at the end of an 18-year rotation on the 5x5 grid points.....	44
<b>Figure 4.9</b> Current and projected probability of <i>Leptocybe invasa</i> infestation over eastern and north eastern South Africa .....	46
<b>Figure 4.10</b> Current and projected probability of <i>Leptocybe invasa</i> infestation over the study site .....	47



## List of Tables

<b>Table 2.1</b> Examples of GCMs used over southern Africa.....	7
<b>Table 2.2</b> Statistical vs dynamic downscaling of GCMs (adapted from Tadross et al., 2011).....	9
<b>Table 3.1</b> The nine GCMs from the CMIP6 used in the WorldClim climate simulations.....	21
<b>Table 3.2</b> List of parameters used in 3PG in Borges <i>et al.</i> , (2012).....	23
<b>Table 3.3</b> r3PG parameters used for <i>Pinus elliottii</i> in this study. <i>Pinus elliottii</i> parameters adapted from Sithole (2011). .....	24
<b>Table 3.4</b> Sites used to verify the performance of the r3PG model prior to use for future projections.....	27
<b>Table 3.5</b> Preferred climate for <i>Leptocybe invasa</i> (sourced from CABI, 2021) .....	32
<b>Table 3.6</b> Bioclimatic variables used in Maxent to calculate <i>Leptocybe invasa</i> risk.....	32
<b>Table 4.1</b> Shifts in the percentage of the area that loses precipitation in RCPs 4.5 and 8.5.....	37
<b>Table 4.2</b> The projected percentage of points belonging to site classes per scenario .....	38
<b>Table 4.3</b> Summary statistics of the plot of modelled versus observed volume .....	40
<b>Table 4.4</b> Changes in average values of stand volume from one of the changing CO <sub>2</sub> test runs with average MAP, MAT and CO <sub>2</sub> across all scenarios .....	41
<b>Table 4.5</b> Percentages of number of points that lost volume and the percentage of total average volume lost by those points for both <i>E. g x u</i> and <i>P. elliottii</i> across all scenarios from the current. ....	42
<b>Table 4.6</b> Percentage of points distributed by percentage of projected <i>Leptocybe invasa</i> risk across all scenarios .....	46

## List of abbreviations and acronyms

AOGCM	Atmospheric and Oceanic Global Circulation Model
AR4	IPCC Assessment Report 4
AR5	IPCC Assessment Report 5
CCAM	Conformal Cubic Atmospheric Model
CMIP5	Fifth Coupled Model Inter-comparison Project
CORDEX	Coordinated Regional Downscaling Experiment
CSIR	Council for Scientific and Industrial Research
CSIRO	Commonwealth Scientific and Industrial Research Organisation
GCM	Global Circulation Model
GHG	Greenhouse gas
IPCC	Inter-governmental Panel on Climate Change
MBM	Mensuration-based growth and yield model
OGCM	Oceanic Global Circulation/Climate Model
PBM	Process-based carbon balance model
RCM	Regional Climate Model
SADC	Southern Africa Development Community
WCRP	World Climate Research Program
<i>E. g x u</i>	<i>Eucalyptus grandis x urophylla</i>
<i>P. elliotii</i>	<i>Pinus elliotii</i>
MaxEnt	Maximum entropy
MAP	Mean annual precipitation
MAT	Mean annual temperature
DEA	Department of Environmental Affairs
KZN	KwaZulu-Natal
RCP	Representative concentration pathway
R3PG	R - Physiological Processes Predicting Growth

# Chapter 1 General overview

## 1.1 Introduction

The integration of site edaphic information such as soil characteristics and potential evapotranspiration in forest stand growth models is gaining traction (Dye, 2001), especially in short rotation *Eucalyptus* growth models (Scolforo *et al.*, 2016; Scolforo, *et al.*, 2019a; 2019b). However, there is a small body of knowledge on how to incorporate short- and medium-term future climate variables into empirical growth equations for clonal eucalypt plantations (Sharma *et al.*, 2015), especially in South Africa. This knowledge could potentially improve the preparedness of the global eucalypt forest industry by advising silvicultural interventions to mitigate and adapt to future climate variability.

Process-based models in which climate and edaphic data are integrated offer a solution (Subramanian *et al.*, 2019). An example of such a model is the well-known 3-PG (Landsberg and Waring, 1997) which besides edaphic information, uses climate data (such as vapour pressure deficit, temperature extremes, precipitation) to estimate biomass, volume and stand basal area. From these information 3-PG calculates the radiant energy absorbed by forest canopies and converts it into biomass production. 3-PG has been parameterized for use in South Africa over the last two decades (Campion *et al.*, 2005; Dye *et al.*, 2004; Esprey *et al.*, 2005), allowing for its application in multi-purpose plantation forests.

Process-based simulation models are very useful tools for exploring potential future growth impacts in terms of all the interacting effects that may come into play. That is, process-based models provide an idea of what forests would look like in different climate scenarios, under potentially varied management and with effects of other risks, like pests, disease, and fire. Quantifying potential future changes in yield and fibre property is of great importance given the likelihood of increasing temperatures in most forestry regions in water-scarce South Africa (Basson, 2011), including projected greater variability in rainfall, with prolonged severe droughts (Department of Environmental Affairs, 2014) and the risk of increased pest and disease infestation (Germishuizen and Mzinyane, 2017). This is especially important for South Africa's plantation forests, which account for approximately half of the total 3.37 million ha of plantation forest in the SADC region (Davis-Reddy and Vincent, 2017) and contribute over USD \$918,000,000 to the country's gross domestic product (Xulu *et al.*, 2019).

South Africa's forest resources in general are vulnerable to the projected climate changes, especially in combination with other factors that interact with climate (Warburton and Schulze, 2008; Xulu et al., 2019). Aspects of climate are important factors in forestry, but their impacts are not always obvious, especially combined with the influence of site-specific characteristics such as altitude and soil type (Naidoo et al., 2013). It is projected that climate change will alter the range limits (growth, survival, and distribution) of current plantation forest tree species due to changing suitability of sites for specific species by climate change (Warburton, 2010). Thus "all-encompassing" forest growth models would offer risk forecasting and contingencies for such an important resource.

The overall goal of this research project was to investigate future climate scenarios projected for the important coastal Zululand region in South Africa and their possible effects on forest plantations. To this end, the research considers both potential gains or losses in productivity as well as risks from changes in pests which may result from changes in climate. The research had four objectives: First, to generate a set of recently updated future climate scenarios for the region. Second, to look at what changes in site characterisation might be expected as an indication of the suitability of the region for current (forestry-based) land uses. Third, to estimate and compare the possible productivity losses or gains for *Eucalyptus grandis x urophylla* and *Pinus elliottii* forest species in the region using a simple process-based model. Last, to overlay a set of likely pest risk scenarios in order to more realistically assess possible yield gains or losses.

## Chapter 2 Literature review

### 2.1 Modelling future climate

Climate change forecasting typically involves use of global circulation models (GCMs) representing physical processes in the atmosphere, ocean, cryosphere, and land surface, simulating the response of the global climate system to increasing greenhouse gas (GHG) concentrations, using different emissions scenarios.

#### 2.1.1 Global scenario of GCMs

Rapid advancements in technology have encouraged the development of more realistic but complex attempts at modelling the earth's climate by incorporating more variables in computations. The Intergovernmental Panel on Climate Change (IPCC) claims to have developed and improved climate models and their simulations since the Fourth Assessment Report (AR4) (Flato *et al.*, 2013) in that respect. Some of the developments include extending models to Earth System Models (ESM) by including the representation of biogeochemical cycles important to climate change (Flato *et al.*, 2013). However, factors such as the immense computational and resource demands that are required to execute ESMs leave GCMs popular. GCMs remain the primary tools available for investigating the response of the climate system to various forcings, for making climate projections. It is therefore crucial to evaluate the performance of GCMs both individually and collectively (Lupo and Kininmonth, 2013). As such the scope of this paper will be limited to GCMs evaluated in the AR5 and those in use in southern Africa.

#### 2.1.2 IPCC AR5

Atmospheric and Oceanic Global Circulation Models (AOGCMs) were the 'standard' climate models assessed in the AR4 (Flato *et al.*, 2013) and continued to be developed and improved in the IPCC's Fifth Assessment Report (AR5). An AOGCMs simulates the dynamics of the physical components of the climate system (atmosphere, ocean, land, and sea ice). This simulation is then used for making projections based on future GHG concentrations and aerosol forcing. In addition, high-resolution or variable-resolution AOGCMs are often used in climate process simulations and result projections with a focus on a particular region.

The AR5 also assessed regional climate models (RCMs) which are limited-area models with representations of climate processes comparable to those in the atmospheric and land surface components of AOGCMs (Flato *et al.*, 2013). An RCM is often used to downscale AOGCMs for some smaller geographical region to provide more detailed information through the

use of limited area physically based models (Giorgi, 2019), and thus are also commonly referred to as [dynamical downscaling](#).

AOGCMS and RCMs assessed in the AR5 stemmed from the Fifth Coupled Model Inter-comparison Project (CMIP5). The CMIP5 was a set of coordinated climate model experiments led by the World Climate Research Program (WCRP). It aimed to perform a suite of climate simulations “that focused on major gaps in understanding of past and future climate changes” (Taylor, et al., 2012, p 485). In a nutshell the project compared the simulation processes and results across a host of AOGCMs (**Figure 2.1**) and RCMs in an attempt to understand the differences in the modelling and predictive capabilities among the AOGCMs. Compared to its predecessors, the CMIP5 included more comprehensive higher-spatial-resolution models, a broader set of experiments, and a richer set of output fields (Braconnot *et al.*, 2011).

### **2.1.3 GHG concentrations in climate models**

Future climate projections in climate models are simulated by representative concentration pathways (RCPs), which model future scenarios of GHG concentrations in the atmosphere. In the AR5 (2014), four pathways were used for climate modelling and research to describe possible climate futures depending on the quantity of GHGs emitted in the next years.

The RCPs were defined by their total radiative forcing<sup>1</sup>, pathway and level by 2100<sup>2</sup>. They describe four different 21st century pathways of GHG emissions and atmospheric concentrations, air pollutant emissions and land use (Collins *et al.*, 2013). The RCPs include a stringent mitigation scenario (RCP2.6), two intermediate scenarios (RCP4.5 and RCP6.0) and one scenario with very high GHG emissions (RCP8.5)<sup>3</sup>. Scenarios without additional efforts to constrain emissions lead to pathways ranging between RCP6.0 and RCP8.5 as shown in **Figure 2.2** (Collins *et al.*, 2013). RCP2.6 is representative of a scenario that aims to keep global warming likely below 2°C above pre-industrial temperatures.

Research on future climates in South Africa (as with most of the world) are mainly based on RCP 4.5 and RCP 8.5. RCP 4.5 describes a future with relatively ambitious emission reductions whereas RCP 8.5 describes a future with no reductions in emissions. Emissions in RCP 4.5 peak

---

<sup>1</sup> cumulative measure of human emissions of GHGs from all sources.

<sup>2</sup> [Representative Concentration Pathways \(RCPs\)](#)

<sup>3</sup>The RCPs are labelled after a possible range of radiative forcing values in the year 2100 (2.6, 4.5, 6, and 8.5 Watts per square metre W/m<sup>2</sup>, respectively)

around 2040, then decline and in RCP 8.5 emissions continue to rise throughout the 21st century (Figure 2.2).

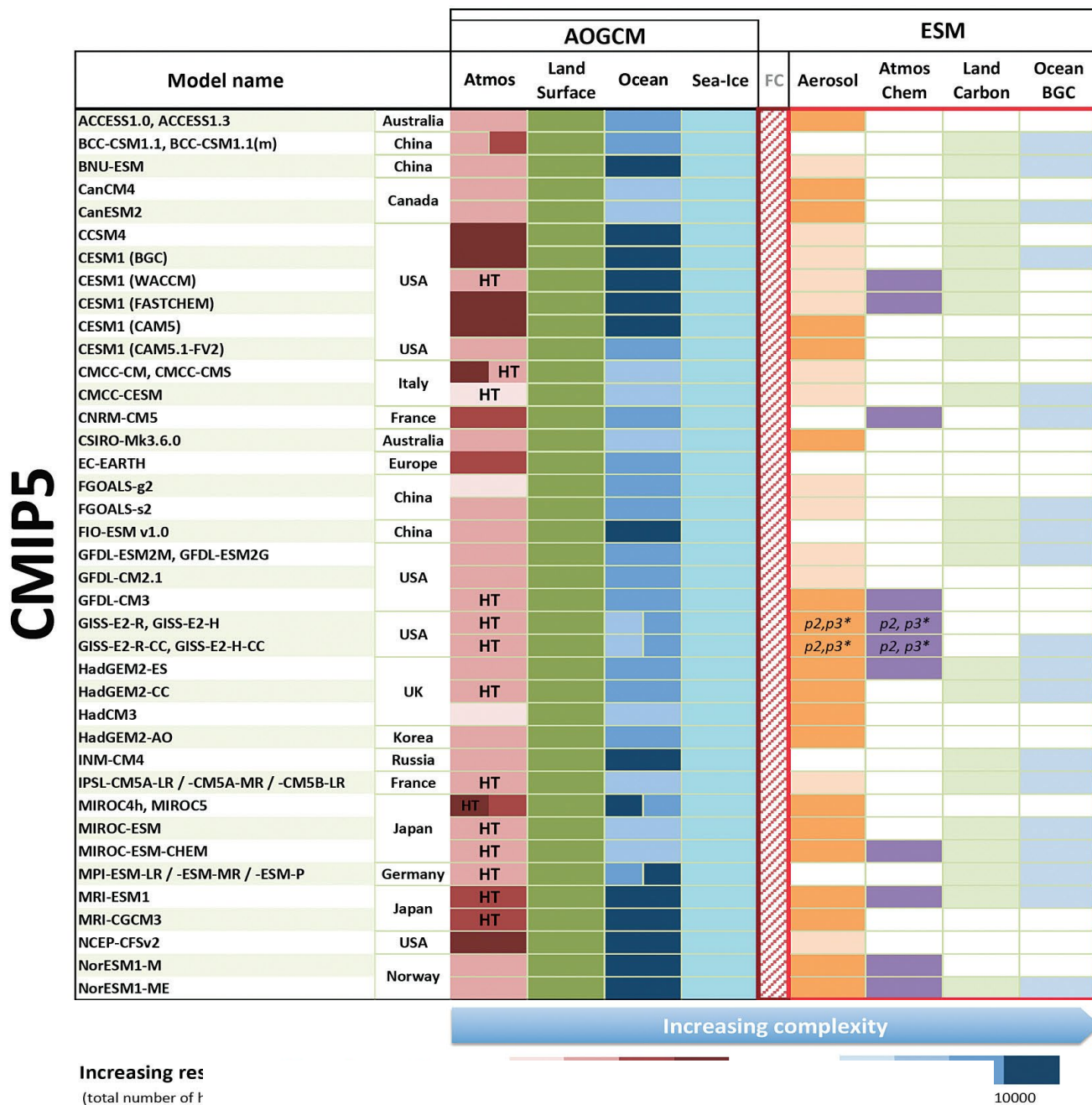
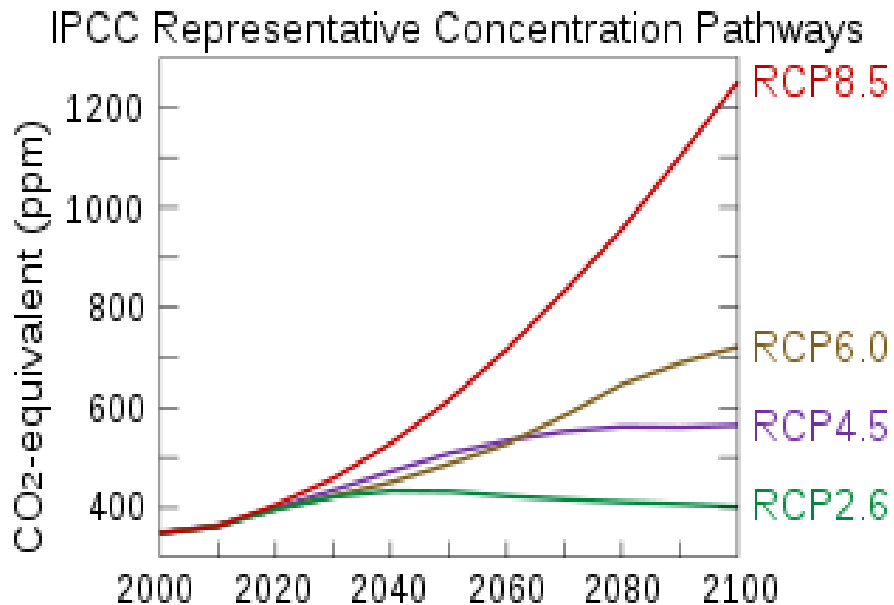


Figure 2.1: GCMs that participated in the CMIP5 experiment (Flato et al., 2013)

## 2.2 GCMs in Southern Africa

Due to the biases and uncertainties associated with a single GCM, climate modelling and projection is expressed either as a range of future changes or as a summary statistic of the distribution of projected changes across number of GCMs (Tadross *et al.*, 2017). A multi-model ensemble approach is taken to describe the range of uncertainty associated with climate change projections (McSweeney *et al.*, 2015). While this does not provide explicit answers, it affords an important perspective on the range of potential climate futures, which are similarly conceivable.

Multi-model ensembles have to conform to conventions set mostly by the IPCC (2014a). As a result, most (if not all) multi-model ensembles of GCMs used in climate simulation and projection in southern Africa have been adapted from the CMIP3 and CMIP5 of the AR4 and AR5 respectively. For instance Engelbrecht *et al.* (2011) downscaled six ensemble GCMs from the CMIP3 using a Conformal Cubic Atmospheric Model (CCAM) to obtain projections of future climate change over southern Africa. Another study used the CCAM to downscale another six CMIP3 GCMs to project surface temperatures over Africa under the A2 scenario of the AR4's Special Report on Emission Scenarios (Engelbrecht *et al.*, 2015). Pinto, *et al.* (2018) downscaled four GCMs from the CMIP5 using two RCMs from the Coordinated Regional Downscaling Experiment (CORDEX) to investigate changes in precipitation and the circulation processes driving them. Some of these GCMs are listed in the **Table 2.1**.



**Figure 2.2:** Representative concentration pathways (RCP) in the AR5 (IPCC, 2014b)



**Table 2.1** Examples of GCMs used over southern Africa

<b>GCM</b>	<b>Country</b>	<b>MIP</b>	<b>Study</b>
<b>CSIRO Mk 3.5</b>	Australia	CMIP3	Engelbrecht <i>et al.</i> , 2011; 2015; Landman <i>et al.</i> , 2018
<b>GFDL2.1</b>	United States	CMIP3	Engelbrecht <i>et al.</i> , 2011; Landman <i>et al.</i> , 2018
<b>GFDL2.0</b>	United States	CMIP3	Engelbrecht <i>et al.</i> , 2011; Landman <i>et al.</i> , 2018
<b>HadCM2</b>	United Kingdom	CMIP3	Engelbrecht <i>et al.</i> , 2011;
<b>HadCM3</b>	United Kingdom	CMIP3	Engelbrecht <i>et al.</i> , 2015; Landman <i>et al.</i> , 2018
<b>CNRMCM5</b>	France	CMIP5	Pinto, Jack and Hewitson, 2018
<b>HadGEM2-ES</b>	United Kingdom	CMIP5	Pinto, Jack and Hewitson, 2018; Dike <i>et al.</i> , 2015
<b>MPI-ESM-LR</b>	Germany	CMIP5	Pinto, Jack and Hewitson, 2018

### 2.3 Downscaling of GCMs

The GCMs in use globally and regionally are usually applied at large spatial scales of about 200-300 km (Flato *et al.*, 2013). They have been found to reliably capture and project changes in temperature. GCMs however fall short in their modelling of changes in rainfall and other climate parameters at the local scale because they often cannot capture a landscape's physical features and processes which are important determinants of local climates (Lupo and Kininmonth, 2013; Tadross *et al.*, 2017). In order to be used at smaller scales (i.e., higher spatial resolutions), these GCMs have to be downscaled to a region of choice. This process allows smaller scale atmospheric, sea and land processes to be represented more realistically. Downscaling translates changes in large-scale atmospheric circulation to finer spatial and temporal scales for use in projections of climate change at local and regional scales. In addition, downscaling accords the validation of model performance and a look at the finer-scale details of GCM projections (Lupo and Kininmonth, 2013).

The process of downscaling usually begins with selecting the appropriate approach; more commonly dynamic or statistical downscaling.

#### 2.3.1 Dynamic downscaling

In dynamic downscaling (DD), a dynamic climate model (either a higher resolution limited-area model or variable resolution global model) is nested within a GCM. The DD uses RCMs driven by GCM output or re-analysis data to produce regionalized climate information (Tang *et al.*, 2016). The outputs from GCMs are used to drive higher resolution RCMs which have a better

representation of local terrain morphology, processes and other conditions (UNEP-DTU and CTCN, 2017).

Downscaling of GCMs to RCMs is often a tricky process as it has to factor in numerous important local processes that determine a region's weather and climate such as terrain formations (topology) that influence convection rainfall. As a result, there are significant levels of uncertainty and numerous scenarios or place-time based contexts. These scenarios vary, with often highly different outcomes that can problematize the derivation of decisive information (UNEP-DTU and CTCN, 2017), with increasing spatial and temporal resolutions.

### **2.3.2 Statistical downscaling**

Statistical downscaling (SD) establishes statistical links between large-scale climate phenomena from GCMs and observed local-scale climate from historical observations (e.g., weather station data). These statistical relationships predict local climate variables (called predictands) (Tang *et al.*, 2016; Najafi and Kermani, 2017). These statistical relationships formed during SD are always needed to correct for biases that occur even in RCMs (UNEP-DTU and CTCN, 2017).

Statistical downscaling is less computationally demanding compared to dynamic downscaling, especially because it barely accounts for some local scale interactions. Perhaps what limits its application in regions like southern Africa is its demand for high-quality observational data (Tadross *et al.*, 2017), which is rare in that part of the world.

Despite the mainly process-linked limitations in downscaling GCMs, there are several advantages from the results of downscaling (see **Table 2.2**). Downscaling offers improved understanding of local future climate conditions and their impacts on landscape resources. For instance, the outputs quantifying climate variables assist in planning for adaptation responses to potential impacts, that are sustainable and appropriate for future climate conditions in the given location (UNEP-DTU and CTCN, 2017). With respect to South African forestry, this translates into improved preparedness (environmental and socio-economical) of the plantation industry to future climate conditions and extremes including floods, droughts and potential site suitability changes (Naidoo *et al.*, 2013). This contributes to minimising losses from and damages to forest plantations resulting from improper adaptation.

## **2.4 Downscaled GCMs in southern Africa**

Detailed localized climate impact and adaptation strategy and policy development are better informed by climate projections that factor in localized processes i.e., downscaling. Progress has

been made towards providing reliable climate change models and predictions for southern Africa by increasing the spatial and temporal resolution of GCMs through downscaling. Here we discuss some of these downscaling efforts and their products, that have found wide use in climate simulations in South Africa and Southern Africa at large.

**Table 2.2** Statistical vs dynamic downscaling of GCMs (adapted from Tadross et al., 2011)

	<b>Statistical (empirical) downscaling</b>	<b>Dynamic downscaling (RCMs)</b>
<b>Advantages</b>	<ul style="list-style-type: none"> <li>• Station scale output</li> <li>• Less computational resources required</li> <li>• Relatively fast (Nikulin <i>et al.</i>, 2018)</li> <li>• Available for more GCMs, allowing an assessment of probabilities and risks</li> <li>• Can be applied to any observed variable, e.g., streamflow</li> </ul>	<ul style="list-style-type: none"> <li>• 10 - 50 km resolution output</li> <li>• Physical interactions and local fine-scale feedback process (not anticipated with statistical methods) can be simulated</li> <li>• Improved simulation of regional climate dynamics</li> <li>• Can include additional processes (large number of variables) not included by the GCM simulations (Nikulin <i>et al.</i>, 2018)</li> <li>• Consistent with GCM simulations</li> <li>• Do not rely on the assumption of stationarity in climate</li> </ul>
<b>Limitations</b>	<ul style="list-style-type: none"> <li>• May not account for some local scale interactions (limited to a few variables), e.g., between the land and the atmosphere</li> <li>• Assumes present-day statistical relationships between synoptic and local-scale climates</li> <li>• Requires the availability of high-quality observational data</li> <li>• Choice of predictor variables can change results</li> <li>• Results do not feed back to the GCM</li> <li>• Choice of statistical transfer scheme can affect results</li> </ul>	<ul style="list-style-type: none"> <li>• Computationally demanding</li> <li>• Only a few scenarios usually developed</li> <li>• Susceptible to the choice of physical parameterisations</li> <li>• Not easily transferred to new regions</li> <li>• Limited regional-to-global feedbacks may be considered, but often are not</li> </ul>

### 2.4.1 CORDEX

The WCRP's Coordinated Regional Climate Downscaling Experiment (CORDEX) aims to foster international collaboration to generate an ensemble of high-resolution historical and future climate projections at regional scale, by downscaling the GCMs participated in the CMIP5 (Dosio and Jürgen, 2016). A lot of the downscaling done using CORDEX produces RCMs with a resolution

of at least 50km (0.44°)<sup>4</sup>. CORDEX RCMs have been found to simulate most timing, intensities and frequencies of rainfall events and their variation over southern Africa quite well (Dosio and Jürgen, 2016; Maure *et al.*, 2018; Pinto *et al.*, 2018; Dosio *et al.*, 2019).

#### **2.4.2 Conformal-Cubic Atmospheric Model (CCAM)**

The Council for Scientific and Industrial Research (CSIR) in South Africa conducted a set of climate simulation experiments where a variable-resolution atmospheric global circulation model (AGCM) was applied as an RCM to simulate climate over Southern Africa (Tadross *et al.*, 2017). The AGCM used to perform the downscalings is the CCAM of the Commonwealth Scientific and Industrial Research Council (CSIRO) in Australia (Mcgregor, 2005). The CCAM is a cube-based global model, semi-Lagrangian, semi-implicit solution of the primitive equations. It employs a Conformal Cubic grid which is realised by projecting a cube onto the surface of a sphere<sup>5</sup>. The simulation, application and validation of the CCAM's downscaling of CMIP5 GCM processes and results over southern Africa have been done in a number of studies by Engelbrecht *et al.* (2011, 2015) and Landman *et al.* (2018). The CCAM's ability to produce data at spatial resolutions of up to 1km (Engelbrecht *et al.*, 2011) make it a good source of information for forestry yield modelling.

### **2.5 A changing climate in southern Africa**

The global climate has undergone significant warming – land, oceanic and atmospheric temperatures have never been higher. The last five years alone have been the warmest on record since 1880<sup>6</sup>. The combined land and ocean surface temperature has warmed by 0.8.5 [0.65 to 1.06] °C from 1880 to 2012. The upper 75 m of the ocean warmed by 0.11 [0.09 to 0.13] °C per decade from 1971 to 2010. It is “*virtually certain*” that the rest of the ocean warmed as well (IPCC, 2014).

Similarly, the average land-surface temperature has increased across Africa, with regions such as southern Africa experiencing greater change (0.4 °C per decade in the last century) than other regions. Observed seasonal temperature trends show a slightly larger warming in summer (DJF) and autumn (MAM) compared with the other seasons (Davis-Reddy and Vincent, 2017). Similarly, sea-surface temperatures (SST) have increased along the southern African coastline.

---

<sup>4</sup> [CORDEX-COMmon Regional Experiment \(CORE\) Framework](#)

<sup>5</sup> [Conformal Cubic Grid](#)

<sup>6</sup> <https://www.noaa.gov/news/2019-was-2nd-hottest-year-on-record-for-earth-say-noaa-nasa>

South Africa's position between the 22° and 35° southern latitudes gives it a predominantly subtropical climate. Its regions experience a variety of weather phenomena mostly due to their fluctuating topography and positions relative to the oceans. This interplay of ocean currents and altitude lead to the spatial, intra-seasonal and inter-annual variation of rainfall and temperature patterns over the country, which could classify the country into vastly different climatological regions.

The southern and eastern escarpments are the regions with the lowest mean temperatures due to the decrease in temperature as the altitude increases while the coastal areas and the interior of the Northern Cape are the warmest areas (Landman *et al.*, 2018). The oceans surrounding South Africa moderate the temperatures experienced along the coastal areas (Engelbrecht *et al.*, 2011). The warm Agulhas Current off the Indian ocean causes the eastern coastal areas to have a warm and humid climate, while the arid climate of the west coast is attributed to the Atlantic ocean's cold Benguela Current (Davis-Reddy and Vincent, 2017). The interaction between the Agulhas Current, moist air from the Indian Ocean, and the eastern escarpment (Simon *et al.*, 2015) results in orographic precipitation over eastern South Africa. There are also pockets of high rainfall along the southwestern Cape and Cape south coast areas, which similarly result from orographic forcing when moist frontal air is transported inland. Therefore, there is a general east-west increase in aridity, with a high spatial rainfall variability over South Africa.

### **2.5.1 Future temperature and rainfall in South Africa**

South Africa is projected to experience an increase in average temperatures between 3 and 7 °C over its interior regions by the end of the century (2080-2100) under RCP 8.5. The least of the temperature increase are expected over the southern interior and coastal areas. This increase in temperature is projected to occur with an increase in the number of very hot days on which the maximum temperature exceeds 35°C.

Rainfall on the other hand is expected to reduce in quantity and increase in variability (Engelbrecht *et al.*, 2011; Engelbrecht, 2019). Over time, changes in rainfall will vary across South Africa between short-medium term and long-term projections. The south-western region of South Africa is projected to have a drying trend (Germishuizen, 2014) that is expected to increase over time which could result in significant reductions in rainfall (Germishuizen and Mzinyane, 2017). In contrast, slight increases in rainfall are projected over parts of the interior of the country with larger

increases towards the north-eastern boundary with Mozambique (Davis-Reddy and Vincent, 2017).

### **2.5.2 Climate in the Zululand region**

Zululand is South Africa's main commercial forestry region (du Plessis and Zwolinski, 2003; Melesse and Zewotir, 2017). It is characterized by a subtropical climate, with mean minimum temperatures of 16°C around June–August and mean maximum of 27°C during November–March (Dlamini *et al.*, 2019, p. 131). The mean annual precipitation ranges between 739 to 1219 mm and peaks during mean maximum temperature (Dube *et al.*, 2015); the mean potential evapotranspiration is commonly in the range of 1100 to 1772mm (Xulu *et al.*, 2019). The landscape consists of Quaternary alluvial sediments of clay sands of aeolian deposits and soil with varying amounts of organic matter, (Nxumalo and Oladele, 2013) at an elevation of 30 to 100 m above sea level. The high penetrability of the soils permits rapid leaching of their nutrients due to the high rainfall. These conditions have been said to be favourable for fast-growing Eucalyptus plantations (Xulu *et al.*, 2019).

Rainfall in Zululand is modulated mainly by interactions of the El Niño-Southern Oscillation (ENSO) and sea surface temperature (SST) anomalies in the southwest Indian Ocean (Nash *et al.*, 2019), with the ENSO being perhaps the more notable determinant of drought occurrence (Thomson *et al.*, 2003; IPCC, 2014; Siderius *et al.*, 2018). Drought conditions prevail typically during the mature El Niño–Southern Oscillation phenomenon when the central and eastern tropical Pacific and the Indian Ocean are warmer than average (Nash *et al.*, 2016). A strong El Niño signal in Zululand has been observed to bring drier conditions which adversely affect forest productivity (Xulu *et al.*, 2019).

During 2015, South Africa received a minimum record 400mm<sup>7</sup> of annual rainfall (lower than the annual average of approximately 730mm), which was preceded by three consecutive years of less-than-normal rainfall (Xulu *et al.*, 2019). This drought stood out as arguably the most extreme and prolonged South Africa (and Zululand) had experienced (Xulu *et al.*, 2019). The 2015 drought led to extensive tree mortality and was a serious setback to forest productivity in Zululand (Xulu *et al.*, 2018). Tree mortality in drought conditions is characterized by insufficient soil moisture to support tree development during the reproductive phase and is the natural outcome of anomalous precipitation deficits and above-normal temperatures (Xulu *et al.*, 2019).

---

<sup>7</sup> <https://www.worldweatheronline.com/ulundi-weather-averages/kwazulu-natal/za.aspx>

Future climates in Zululand are projected to become more adverse. Predictions indicate reductions in rainfall and increases in its variability and drought occurrences (De Cauwer *et al.*, 2018; Xulu *et al.*, 2018, 2019). The increased duration, frequency and magnitude of drought in Zululand could have serious impacts on forests (Bond *et al.*, 2020), even more so when combined with high-intensity fires commonly associated with drought conditions.

## 2.6 Forestry in the Zululand coastal plain

South Africa's coastal Zululand is home to some of the country's most productive eucalypt forest plantations. When compared to other species such as pine, *Eucalyptus* is generally fast growing, has a higher yield, wider range of uses and has a shorter rotation age (Lu *et al.*, 2020). To increase the resilience of the valuable crop to fungi, diseases and pests in Zululand – characterized by having a sub-tropical climate (Abraha and Savage, 2006). *Eucalyptus grandis*, previously an industry mainstay, has largely been replaced in Zululand with the clonal hybrid *E. grandis* x *E. urophylla* (*E. g x u*). The *E. g x u* hybrid is a mesh of the *E. urophylla*'s high wood density, disease tolerance and survival and the *E. grandis*' fast-growing properties (Melesse and Zewotir, 2017). These characteristics have made the *E. g x u* essential among South African pulp, paper, timber and biorefinery industries (Mphahlele *et al.*, 2021).

A factor of concern to commercial forest managers is unpredictable climate change, which affects the productivity of forest crops. Climate change particularly in coastal Zululand is projected to take the form of increased temperatures, reduced (and increased)<sup>8</sup> precipitation (Engelbrecht, 2019; Tadross *et al.*, 2017) with increased variability and increased atmospheric CO<sub>2</sub> concentration (Germishuizen and Mzinyane, 2017). The physiological responses of trees to such possible climate changes are uncertain but they are likely to be site and species specific (Warburton and Schulze, 2006; Naidoo, Davis and van Garderen, 2013). As such, climate risk assessment tools integrated with process-based models have never been more critical. The benefit of such a system is to greatly improve forest planning, monitoring and management (Elli, 2020). This is more so important in water scarce South Africa (Department of Environmental Affairs, 2014), that historically has had severe droughts in the past that affected forestry in sub-tropical Zululand as well (Crous *et al.*, 2013; Xulu *et al.*, 2018).

---

<sup>8</sup> With reference to the extent of the study area, while some areas are projected to receive less precipitation, others may experience an increase (see Davis-Reddy and Vincent, 2017; Warburton and Schulze, 2008)



According to Bréda and Brunette (2019) short-term rotations (such as in coastal Zululand) can give the best economic return on forest investment as a solution to mitigate the impacts of drought events. Nonetheless, the impact of drought on short-rotation commercial forestry can still be long-term, cost-expensive and irreversible (Warburton and Schulze, 2006). For instance, studying five *Eucalyptus* genotypes in KwaZulu-Natal, Crous et al. (2013) mention that in the absence of large-scale management interventions such as irrigation and thinning, stand volume growth rate in water-limited scenarios decreases with an increase in stand density over time resulting in a convergence of stem growth within certain limits of stand densities. Du Plessis and Zwolinski (2003) agreed that climate fluctuations can have a profound impact on the behavioral growth pattern of short-rotation eucalypt stands. Additionally, because of drought, tree planting might be seriously affected which also warrants the need for much more frequent blanking. This emphasizes the need to model and forecast the long-term and large-scale responses of short-rotation forestry to projected estimated future climates to plan and inform management interventions.

## 2.7 Physiological Processes Predicting Growth (3-PG) Forest Growth Model

Developed by Landsberg and Waring (1997), 3-PG (Physiological Processes Predicting Growth) is a process-based, stand-level model of forest growth applicable to plantations, or to even-aged, relatively homogeneous forests. It is an attempt to bridge the gap between conventional empirical, mensuration-based growth and yield models, and process-based, carbon-balance models (Sands, 2003). Since its development, the model has been parameterised and tested in different countries and regions for different species as both a research and operational tool and published widely (see [3-PG studies](#)<sup>9</sup> and Gupta and Sharma, 2019a).

The 3-PG model simulates the development of a forest stand via five submodules: biomass production (light), biomass allocation, soil water balance, stem mortality and stand characteristics. Details on the processes, equations and principles that the construction of the submodules are based on can be found in (Landsberg and Waring, 1997; Sands and Landsberg, 2002; Almeida, 2003; Sands, 2003; Landsberg and Sands, 2011).

In the biomass submodule, species-specific light extinction coefficients and leaf area index (LAI) are combined to calculate the light absorbed by the canopy using Beer's law (see Pfeiffer and Herman, 1943). The gross primary production (GPP) is based on a species-specific canopy

---

<sup>9</sup> <https://3pg.forestry.ubc.ca/3pg-studies/>



quantum efficiency ( $\alpha_c$ ) that is dependent on factors such as temperature, frost, vapour pressure deficit (VPD), soil characteristics and atmospheric CO<sub>2</sub> (Sands and Landsberg, 2002; Trotsiuk *et al.*, 2020). GPP is then multiplied by a constant carbon use efficiency factor to derive Net primary productivity (NPP), which is allocated to the roots, stem and foliage respectively influenced by soil nutrients and moisture, VPD and tree size. In the water submodule (soil water balance), tree transpiration and soil evaporation are calculated using the Penman–Monteith equation. These results are combined with canopy interception to predict evapotranspiration.

The mortality sub-model calculates density-independent mortality caused by pests or drought for instance, and density-dependent mortality based on Yoda's  $-3/2$  self-thinning law (see Mrad *et al.*, 2020). After each monthly time step, the stand characteristics submodule uses allometric relationships (introduced in the Fortran and r versions of 3PG (Trotsiuk *et al.*, 2020)) to convert biomass into output variables of interest such as mean diameter, basal area, and volume.

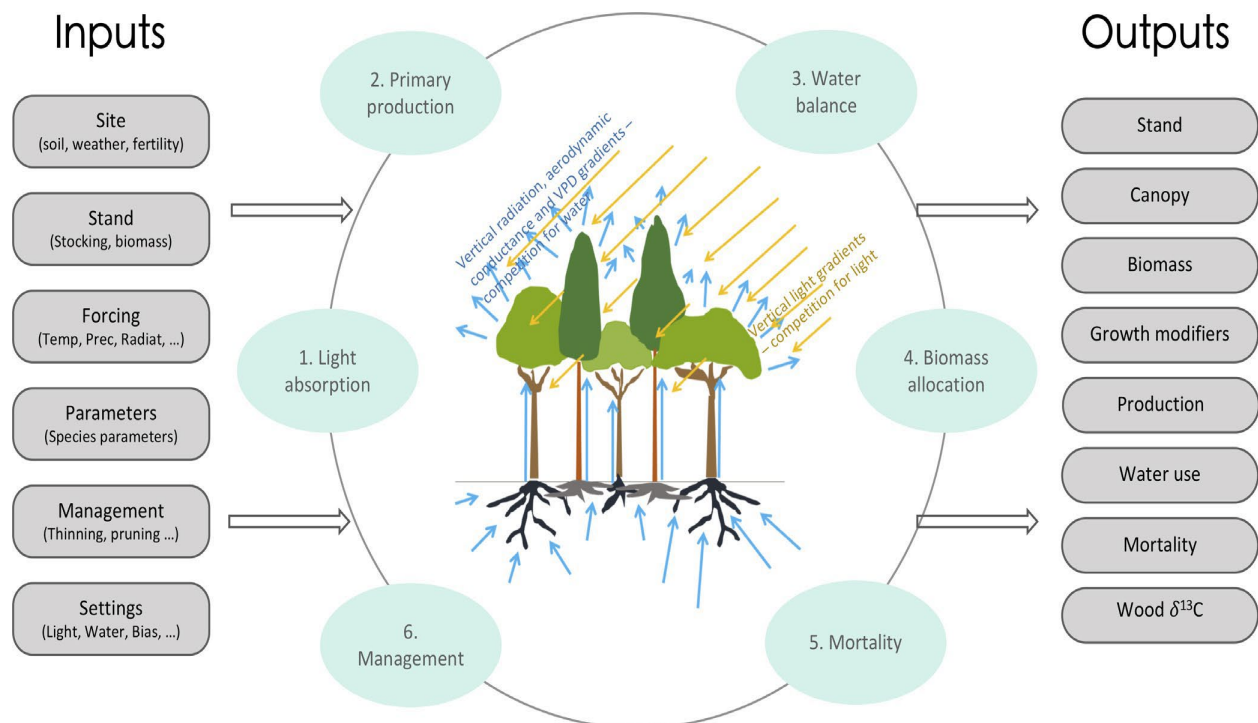


**Figure 2.3:** The structure of the 3-PG model according to Trotsiuk *et al.* (2020)

3PG requires monthly average values of solar radiation, mean air temperature, atmospheric vapour pressure deficit, rainfall, and frost days as climatic inputs (Sands, 2003). The other inputs into the model are site-specific: position relative to the equator (latitude), maximum available soil water, soil texture and a site fertility rating.

Numerous studies have applied 3PG to *Eucalyptus* genotypes in different ways. Stape et al., (2004) calibrated 3PG for use in an irrigated plantation in Brazil to simulate the response of *Eucalyptus grandis x urophylla* to changes in soil fertility. In Australia, 3PG was used to predict above- and below-ground biomass estimates from carbon sequestration by *Eucalyptus cloeziana*, *Eucalyptus argophloia* (besides one Acacia and two Pine species) for a range of different soil productivity conditions. In South Africa, Dye et al. (2004) concluded that 3PG could realistically simulate growth and water use over a wide range of rotation age and growth conditions in *Eucalyptus* plantations. 3PG's responsivity to a wide range of input parameters such as soil, climate, initial stand conditions and silvicultural treatments has made it very useful for the estimation of wood formation during short rotations especially where a few years of unusual weather may strongly influence growth and yield (Scolforo, et al., 2019; Stape et al., 2004). The wide adoption of the 3PG model can be attributed to its simple structure, free source code, relatively few input parameters including probable silvicultural treatments and ability to integrate spatial data. As observed in the previously mentioned literature, 3PG also allows for parameterization for individual species.

### **2.7.1 Effect of atmospheric CO<sub>2</sub> concentration on tree growth and 3PG modelling**

Atmospheric carbon dioxide (CO<sub>2</sub>) is important in plant photosynthetic and biomass production processes. The CO<sub>2</sub> fertilization hypothesis stipulates that rising atmospheric CO<sub>2</sub> has a positive effect on net primary productivity (NPP) in plant processes due to the increasing availability of carbon (Girardin *et al.*, 2011; Walker *et al.*, 2021). This concept has had a long experimental theory in several laboratory conditions as well as free-air CO<sub>2</sub> enrichment (FACE) studies (Norby and Zak, 2011). Studies on the effect of rising atmospheric CO<sub>2</sub> on forests have also shown that there is a positive correlation between CO<sub>2</sub> and stomatal conductance and plant water use efficiency (Almeida et al., 2009). Thus, it is important to consider the effect of CO<sub>2</sub> in tree physiological processes that determine yield.

However, studies have inconclusive findings on the effect of increasing atmospheric CO<sub>2</sub> concentrations on intrinsic water use efficiency iWUE, plant stomatal conductance and plant growth (Walker *et al.*, 2021). For instance Peñuelas, Canadell and Ogaya, (2011) found that tree growth did not increase in tropical biomes as expected despite increase in atmospheric CO<sub>2</sub> concentrations 40 years prior to the year of their study. Similarly, Norby et al. (2021) found little evidence that elevated CO<sub>2</sub> accelerated tree and stand development in a 12-year experiment that investigated forest canopy development and stand growth indicators such as basal and height. Wang and Feng (2012) found no significant relationship between precipitation and plants' iWUE

response to increasing atmospheric CO<sub>2</sub>, which probably explains why stand volume kept increasing despite reducing precipitation in our model tests. Contrastingly a study by Girardin et al. (2011) for instance found that there is some fertilization effect of long term CO<sub>2</sub> but up to a certain limit (see also Seely et al., 2015), in line with several studies that generally found that the increased tree growth could diminish over time in the long term potentially leading to early mortality (see Ortega, 2020<sup>10</sup>).

Collectively, the body of literature warns against considering the effects of CO<sub>2</sub> on tree growth in a changing climate because of the uncertainty about its interaction with other factors, including temperature, rainfall distribution and soil fertility (ABARES, 2011). Therefore, the atmospheric CO<sub>2</sub> used in our analyses was kept constant across all the scenarios. Only the effects of estimated future solar radiation, MAT and MAP on stand volume were investigated in the study.

---

<sup>10</sup> Ortega, R. P. (2020). Trees Are Growing Fast and Dying Young Due to Climate Change. *Smithsonian Magazine*. <https://www.smithsonianmag.com/smart-news/trees-are-growing-fast-and-dying-young-due-climate-change-180975819/> Accessed on 19<sup>th</sup> December, 2021

## Chapter 3 Materials and methods

### 3.1 Study area

This study used a set of future climate projections for a set of grid points in a region along the eastern coast of South Africa, in KwaZulu-Natal Province (often referred to as coastal Zululand). The region was created by delineating an approximately 40km inland buffer from Zululand coast, located between longitudes 31.20° E and 32.4.5° E and latitudes 27.825° S and 29.25° S (Figure 1). The region has subtropical latitudes and is characterised by hot and humid summers occurring between October and April, and dry mild winters the rest of the year. The main long-term land uses in coastal Zululand are forestry and sugar cane (Goble and Elst, 2012; Jewitt *et al.*, 2015). It gets most of its precipitation during the summer months with a mean annual precipitation (MAP) of between 739 – 1219 mm (Xulu *et al.*, 2019) and mean annual temperature (MAT) of 22°C (Dovey *et al.*, 2011; Xulu *et al.*, 2018). The areas closest to the coast tend to have greater climate influences from the Indian ocean. Mean annual precipitation (MAP) is decreases rapidly with increasing distance from the coast and from south to north (Gardner *et al.*, 2007). Simultaneously, MAT increases from south to north (du Plessis and Zwolinski, 2003). The soils in the region are predominantly sandy although clay content increases away from the coast (du Plessis and Zwolinski, 2003). The altitude in the study region varies between 3 – 516 m above sea level (KZN Department of Agriculture, n.d.), with the general transition from high to low altitudes occurring from west towards the coast in the east.

Protected and conservation areas<sup>11</sup>, urban areas, and other land uses that could not be used for plantation forestry based on the Protected Area Register of the Department of Environmental Affairs (DEA) <sup>12</sup> were clipped from the region. A 5km x 5 km point grid was created using the 'Create Fishnet' tool in version 10.8 of the ArcGIS <sup>13</sup> Data Management Toolbox (ESRI, Redlands). The scale was determined based on the dataset to be incorporated in the analyses

---

<sup>11</sup> [https://egis.environment.gov.za/protected\\_areas\\_register](https://egis.environment.gov.za/protected_areas_register) accessed on 12-04-2021

<sup>12</sup> [Protected Areas Register \(PAR\) website](#)

<sup>13</sup> ESRI 2020. ArcGIS Desktop: Release 10.8. Redlands, CA: Environmental Systems Research Institute

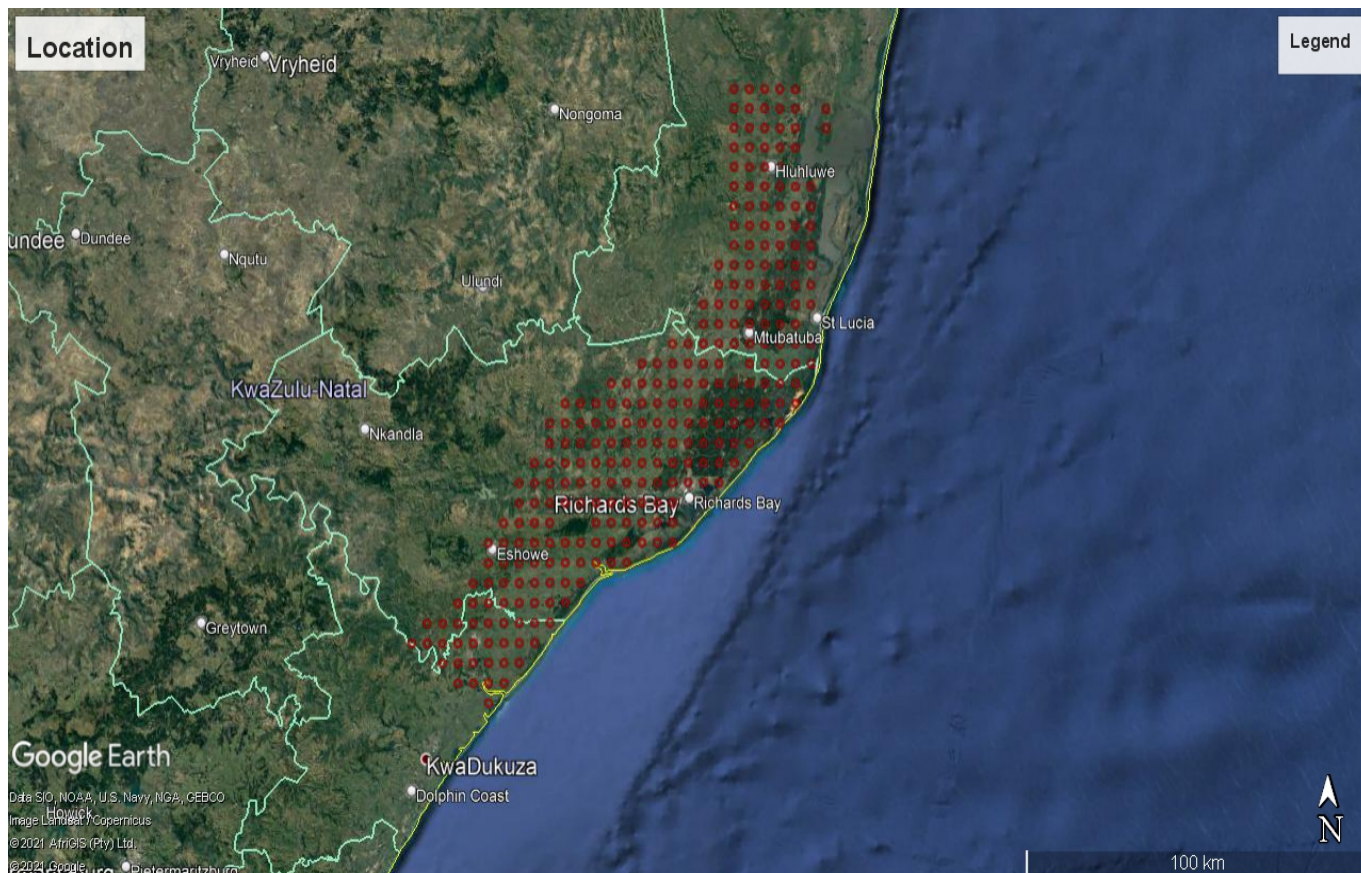


**Figure 3.1:** Location of the study area over coastal Zululand. The red circles represent the 5x5 km point grid for which future climate projections were obtained.

with the lowest spatial resolution. The CMIP6 raster climate data had the lowest spatial resolution (2.5 minutes or 5x5 km). Data from the other datasets incorporated in the analyses were extracted using the 5x5 point grid.

### 3.2 Climate for long term projection models

For long term projections using growth models, data from various Global Circulation Models (GCM) were used. The weather simulated by GCMs depends in part on the assumed atmospheric concentration of greenhouse gases. Representative Concentration Pathways (RCP) describe projected future atmospheric concentrations of greenhouse gases (GHG) based on scenarios that include time series of emissions and concentrations of the full suite of Greenhouse Gases (GHG) (gases that trap heat in the atmosphere) and aerosols and chemically active gases, as well as land use/land cover (Moss et al., 2008). Each RCP provides only one of many possible scenarios that would lead to the specific radiative forcing characteristics. Thus, projected climate for a given period in the future depends on the GCM ensemble and the RCP used.



Four RCPs produced from Integrated Assessment Models were selected from the published literature on phase 6 of the Coupled Model Intercomparison Project (CMIP6) (IPCC, 2014). The RCPs are used in the Fifth Assessment Report (AR5) of the Intergovernmental Panel on Climate Change (IPCC) of the United Nations. The global and regional climate projections are presented by Working Group I (WGI) in Chapters 11 to 14 of the AR5 report (Christensen *et al.*, 2013; Collins *et al.*, 2013; Kirtman *et al.*, 2013; Church and Gregory, 2019).

The climate models used in this study were selected as they are the most recently published set of data easily accessible via the WorldClim website. They are all fully coupled global climate models with atmosphere, ocean, land surface and sea ice components, interacting with each other. Each of the climate models are physically coupled through fluxes of momentum, energy, and water at their interfaces (Wu *et al.*, 2019). The coupling was realized using the flux coupler version 5 developed by the National Center for Atmosphere Research (NCAR).

The climate variables used in this research were based on the climate ensemble calculated as the median of nine GCMs (**Table 3.1**), which provides a more robust estimate of the projected climate than the individual models. The data were monthly average values of minimum temperature (*tmp\_min*), maximum temperature (*tmp\_max*), precipitation (*prcp*), and solar radiation (*srad*) which were processed for nine GCMs **Table 3.1**. These monthly climate figures were repeated each year within a 20-year period. To stay up-to-date or use the most current data readily available, the GCM ensemble was from the CMIP6 which as of March 2021 (the month of the analyses) were only available in the lowest spatial resolution of 2.5-minute spatial resolution (5km x 5km). Therefore, the spatial resolution of the climate data was 2.5 minutes.

The climate data downloaded was projected for RCP4.5 and RCP8.5 (which correspond to Shared Socioeconomic Pathways (SSP) 24.5 and 58.5 respectively), both for the periods 2041-2060 and 2081-2100 i.e., a total of four scenarios. The current climate (1970-2000) was also acquired from the WorldClim website (Fick and Hijmans, 2017).

In most climate studies, the sophistication within and the structural differences across different GCMs have been noted as major sources of uncertainty and inaccuracy. That is why an ensemble of GCMs is used to mitigate these culminating complexities in representing and predicting future climate. The uncertainties from or limitations of the use of GCMs are mostly due to, for instance, unknown future greenhouse gas emissions (due to unknown SSPs or future

human behaviour patterns), errors in the model design or structural model limitations (Elli *et al.*, 2020).

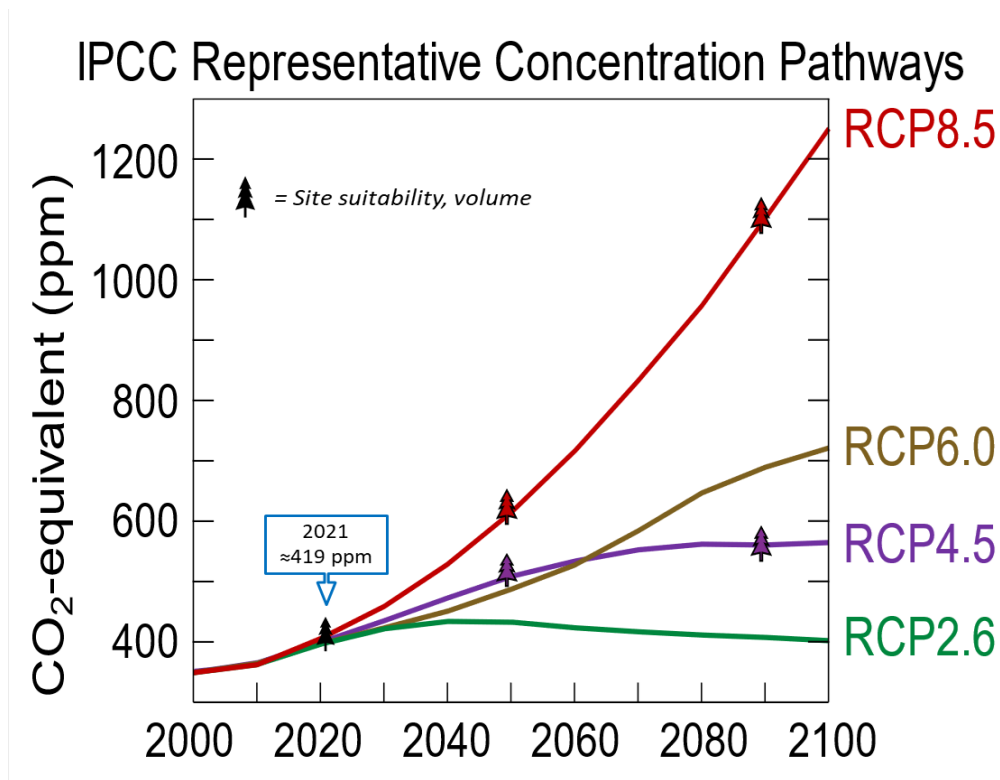


Figure 3.2: RCPs considered in this study and the scenarios along those RCPs (IPCC, 2014b)

Table 3.1 The nine GCMs from the CMIP6 used in the WorldClim climate simulations

Model	Full name	Country of origin
BCC-CSM2-MR	Beijing Climate Centre Climate System Model	China
CNRM-CM6-1	Centre National de Recherches Meteorologiques Climate Model	France
CNRM-ESM2-1	Centre National de Recherches Meteorologiques, France Earth System Model 2	France
CanESM5	Canadian Earth System Model version 5	Canada
GFDL-ESM4	Geophysical Fluid Dynamics Laboratory Earth System Model 4	United States of America
IPSL-CM6A-LR	Institut Pierre Simon Laplace -Climate Modelling – Low Resolution	France
MIROC-ES2L	Model for Interdisciplinary Research on Climate, Earth System version 2 for Long-term simulations	Japan
MIROC6	Model for Interdisciplinary Research on Climate	Japan
MRI-ESM2-0	Meteorological Research Institute Earth System Model version 2.0	Japan

### 3.3 Soils

The soil data for the model projections were extracted from the Schulze (2007) soils database. 3PG uses four soil classes; sandy, sandy loam, clay loam and clay (Sands, 2010). To convert or reclassify the soils data from Schulze (2007) for input into r3PG, the proportion of clay, sand, loam, and their combinations were calculated using a threshold of more than 60%. The soil class that was most dominant in a Schulze soil combination was the designated class for input into 3PG.

The weighted averages of the minimum available soil water (*asw\_min*), initial available soil water (*asw\_i*) and maximum available soil water (*asw\_max*) were calculated based on the depth of the soil horizons (Louise Warburton, personal communication<sup>14</sup>). The *asw\_min*, *asw\_i* and *asw\_max* were identified in the attribute table of the soils database as

- the wilting point (**WP**) of the soil = *asw\_min*; when the soil still contains some water but it is too little for the plant to extract (Lopez and Barclay, 2017)
- the field capacity (**FC**) of the soil = *asw\_i*; where the macropores of soil are filled with both air and water while the smaller pores are still full of water after drainage by gravity action (de Oliveira *et al.*, 2015). At field capacity, the water and air contents of the soil are considered to be ideal for tree growth.
- the point of saturation or total porosity (**PO**) = *asw\_max*; the percentage soil volume occupied by voids (Schulze, 2007) and as such the point at which all the pores in the soil are filled with water (Bordoni *et al.*, 2018)

In the attribute table of the soils data, the soil water variable *WP*, *FC* or *PO* of a point of  $id = n$  at a location  $(x, y)$  was a weighted average calculation involving the depth of soil horizon  $a$  or  $b$  such that

$$Water_{n(x,y)} = \frac{(water_a \times depth_a) + (water_b \times depth_b)}{depth_a + depth_b}$$

Where  $water = WP (asw\_min), FC(asw\_i) \text{ or } PO(asw\_max)$ ;  $depth_a = \text{depth of soil horizon } a$  and  $depth_b = \text{depth of soil horizon } b$  at  $n$ . These *asw* values were calculated for input into r3PG. The grid points were used to extract the from the Schulze (2007) soils data.

---

<sup>14</sup> Personal communication on May 25, 2021.



**Table 3.2** List of parameters used in 3PG in Borges *et al.*, (2012)

Parameter	symbol	Unit	F	C1
Ratio of foliage:stem partitioning at Diameter = 2 cm	pFS2	-	O	1.64
Ratio of foliage:stem partitioning at Diameter = 20 cm	pFS20	-	A	0.15
Constant in stem mass and diameter relationship	stemConst	-	O	0.020
Power in stem mass and diameter relationship	stemPower	-	O	3.11
Maximum fraction of NPP to roots	pRx	-	L	0.5
Minimum fraction to NPP to roots	pRn	-	L	0.1
Maximum litterfall rate	gammaFx	1/month	A	0.07
Litterfall rate for very young stands	gammaF0	1/month	P	0.001
Age at which litterfall rate = $\frac{1}{2}(\gamma F0 + \gamma F1)$	tgammaF	month	A	4
Average monthly root turnover rate	Rttover	1/month	A	0.025
Minimum, optimum and maximum temperature for growth	Tmin/ Topt/ Tmax	°C	L	8/25/40
Value of 'm' when FR = 0	m0	-	P	0
Value of <i>fN</i> when FR = 0	fN0	-	L	0.5
Power of (1 – FR), in the <i>fN</i> expression	fNn	-	L	1
Parameter related with soil water availability	Soil Class	-	O	C
Maximum age of the “stand” to compute relative age	MaxAge	year	L	9
Power of the relative age in the function for <i>fage</i>	nAge	-	P	4
Relative age to reach <i>fage</i> = 0,5	rAge	-	P	0.95
Specific leaf area for initial age planting	SLA0	m <sup>2</sup> kg <sup>-1</sup>	O	13.74
Specific leaf area for adult age planting	SLA1	m <sup>2</sup> kg <sup>-1</sup>	O	7.56
Age which the specific leaf area = $\frac{1}{2}(\sigma_0 + \sigma_1)$	tSLA	year	O	1.23
Extinction coefficient for absorption of PAR by canopy	k	-	P	0.5
Age at canopy cover	fullCanAge	year	O	2
Maximum proportion of rainfall intercepted by canopy	MaxIntcptn	-	P	0.15
LAI for maximum rainfall interception	LAlmaxIntcptn	m <sup>2</sup> m <sup>-2</sup>	L	3.33
Canopy quantum efficiency	Alpha	-	A	0.08
Ratio NPP/GPP	Y	-	L	0.5
Maximum canopy conductance	MaxCond	m s <sup>-1</sup>	P	0.02
LAI for maximum canopy conductance	LAlgcx	m <sup>2</sup> m <sup>-2</sup>	P	3.33
Defines stomatal response to the atmospheric vapour pressure deficit	CoeffCond	mbar <sup>-1</sup>	L	0.0324
Canopy boundary layer conductance	BLcond	m s <sup>-1</sup>	P	0.2
Maximum stem mass per tree	wSx1000	kg tree <sup>-1</sup>	P	300
Branch and bark fraction for initial age plantings	fracBB0	-	O	0.59
Branch and bark fraction for mature stands	fracBB1	-	O	0.19
Age which the branch and bark fraction = $\frac{1}{2}(PBB0+ PBB1)$	tBB	year	O	2.17
Minimum basic density – for young trees	rhoMin	t m <sup>-3</sup>	O	0.382
Maximum basic density – for older trees	rhoMax	t m <sup>-3</sup>	O	0.505
Age which the basic density = $\frac{1}{2}(\rho_0 + \rho_1)$	tRho	year	O	2.264
Constant of the relation between Height vs dbh	aH	-	O	0.67
Power of the relation between Height vs dbh	nHB	-	O	1.27
Constant of the relation between Volume vs dbh	aV	-	O	0.0256
Power of the relation between Volume vs dbh	nVB	-	O	3.22

F = way of obtaining the parameters; O = observed; L = literature; P = Standard (original model); A = adjusted (calibration); C1 = parameters of the model adjusted for the Cerrado; C = indicates the textural class of the soil (clayey); LAI = leaf area index; PAR = photosynthetically active radiation.

### 3.4r3PG runs and parameter assumptions

For this study the simulation runs and optimization were undertaken using 3PG implemented as an R package (*r3PG*) developed by (Trotsiuk *et al.*, 2020) in R (R Core Team, 2021). In addition

to runs for *E. g x u* using parameters in **Table 3.2**, to create a comparison and assess the possible differences in future *E. g x u* growth with another feasible species, a parallel set of runs were undertaken using parameters for *P. elliotii* (Sithole, 2011) (**Table 3.3**). This was done in an attempt to explore alternatives to a possibly unfavourable future for *E. g x u*. Among the criteria that guided the selection of *P. elliotii* (Section 3.6) from the plethora of commercial forest species in South Africa, the most important criterion was the availability of published species parameters for 3PG.

**Table 3.3** r3PG parameters used for *Pinus elliotii* in this study. *Pinus elliotii* parameters adapted from Sithole (2011).

Parameter description	In r3PG	Units	<i>Eucalyptus grandis x urophylla</i>	<i>Pinus elliotii</i>
Foliage: stem partitioning ratio @ D=2 cm	pFS2	-	1.64	0.93
Foliage: stem partitioning ratio @ D=20 cm	pFS20	-	0.15	0.2
Constant in the stem mass v. diam. Relationship	aWS	-	0.099	0
Power in the stem mass v. diam. Relationship	nWS	-	2.506	0
Maximum fraction of NPP to roots	pRx	-	0.5	0.8
Minimum fraction of NPP to roots	pRn	-	0.1	0.25
Maximum litterfall rate	gammaF1	1/month	0.07	0.037
Litterfall rate at t = 0	gammaF0	1/month	0.001	0.001
Age at which litterfall rate has median value	tgammaF	month	4	24
Average monthly root turnover rate	gammaR	1/month	0.025	0
Minimum temperature for growth	Tmin	Deg. C	8	4
Optimum temperature for growth	Topt	Deg. C	25	23
Maximum temperature for growth	Tmax	Deg. C	40	35
Days production lost per frost day	kF	days	0	1
Moisture ratio deficit for f $\theta$ = 0.5	SWconst	-	0.7	0.5
Power of moisture ratio deficit	SWpower	-	9	5
Value of modifier of quantum efficiency at 700 ppm	fCalpha700	-	1.4	0
Value of modifier of canopy conductance 700 ppm	fCg700	-	0.7	0
Value of 'm' when FR = 0	m0	-	0	0
Value of 'fNutr' when FR = 0	fN0	-	0.6	1
Power of (1-FR) in 'fNutr'	fNn	-	1	0
Maximum stand age used in age modifier	MaxAge	years	9	80
Power of relative age in function for fAge	nAge	-	4	4
Relative age to give fAge = 0.5	rAge	-	0.95	0.95
Mortality rate for large t	gammaN1	%/year	0	0.01
Seedling mortality rate (t = 0)	gammaN0	%/year	0	0.15
Age at which mortality rate has median value	tgammaN	years	0	0.5
Shape of mortality response	ngammaN	-	1	1
Max. stem mass per tree @ 1000 trees/ha	wSx1000	kg/tree	300	340

Parameter description	In r3PG	Units	<i>Eucalyptus grandis x urophylla</i>	<i>Pinus elliottii</i>
Power in self-thinning rule	thinPower	-	1.5	1.5
Fraction mean single-tree foliage biomass lost per dead tree	mF	-	0	0
Fraction mean single-tree root biomass lost per dead tree	mR	-	0.2	0.2
Fraction mean single-tree stem biomass lost per dead tree	mS	-	0.2	0.2
Specific leaf area at age 0	SLA0	m <sup>2</sup> /kg	13.74	5
Specific leaf area for mature leaves	SLA1	m <sup>2</sup> /kg	7.56	5
Age at which specific leaf area = (SLA0+SLA1)/2	tSLA	years	1.23	2.5
Extinction coefficient for absorption of PAR by canopy	k	-	0.5	0.5
Age at canopy cover	fullCanAge	years	2	0
Maximum proportion of rainfall evaporated from canopy	MaxIntcptn	-	0.15	0.13
LAI for maximum canopy conductance	LAImaxIntcptn	-	3	8
Alpha	alphaCx	molC/molPAR	0.08	0.05
Ratio NPP/GPP	Y	-	0.5	0.47
Maximum canopy conductance	MaxCond	m/s	0.02	0.02
LAI for maximum canopy conductance	LAIgcx	-	3.33	3.33
Defines stomatal response to VPD	CoeffCond	1/mBar	0.0324	0.05
Canopy boundary layer conductance	BLcond	m/s	0.2	0.2
Branch and bark fraction at age 0	fracBB0	-	0.59	0.75
Branch and bark fraction for mature stands	fracBB1	-	0.19	0.19
Age at which fracBB = (fracBB0+fracBB1)/2	tBB	years	2.17	5
Minimum basic density for young trees	rhoMin	t/m <sup>3</sup>	0.382	0.36
Maximum basic density for older trees	rhoMax	t/m <sup>3</sup>	0.505	0.4
Age at which rho = (rhoMin+rhoMax)/2	tRho	years	2.264	7
Constant in stem height relationship	aH	-	0.67	0.21
Power of DBH in stem height relationship	nHB	-	1.27	1.224
Constant in the stem volume relationship	aV	-	0	9.848
Power of DBH in the stem volume relationship	nVB	-	0	3.381
Intercept of net v. solar radiation relationship	Qa	W/m <sup>2</sup>	-90	-90
Slope of net v. solar radiation relationship	Qb	-	0.8	0.8
Molecular weight of dry matter	gDM_mol	gDM/mol	24	24
Conversion of solar radiation to PAR	molPAR_MJ	Mol/MJ	2.3	2.3

### 3.4.1 r3PG model validation

Initially, general performance of the 3PG model was verified against data from 18 study sites (**Table 3.4** and **Figure 4.6**). Measurements of DBH, tree height and stem numbers from these sites were used to estimate quadratic mean DBH ( $D_q$ , cm) (**Equation 3.1**), Basal area (BA) ( $m^2/ha$ ) (**Equation 3.2**), and stand volume ( $V$ ,  $m^3/ha$ ) using a stand volume estimator by Burkhardt

and Tomé (2012) (**Equation 3.3**). The model was run for parameters published for *E. g x u* by Borges et al., (2012) in **Table 3.2**.

$$D_q = \sqrt{\frac{\sum DBH^2}{n}} \quad \text{Equation 3.1}$$

$$BA = \frac{\pi \cdot (D_q)^2 \cdot TPH_i}{40000} \quad \text{Equation 3.2}$$

$$V = BA \cdot H_{mean} \cdot f \quad \text{Equation 3.3}$$

Where  $V$  is utilisable volume/ha ( $m^3/ha$ ),  $BA$  the basal area ( $m^2/ha$ ),  $D_q$  is the quadratic mean DBH (cm),  $DBH$  is the stem diameter at breast height (cm),  $n$  is the number of observed trees per plot,  $TPH_i$  is number of stems (t/ha),  $H_{mean}$  the mean stand height (m), and  $f$  the species-specific form factor for *E. grandis x urophylla* by (Kassier, 2005).

This stand volume equation was used throughout the study, including for the derivation of volume from simulated BA and height.

In Microsoft Excel, the observed volume and age of rotation for each compartment in **Table 3.4** were recorded. Thereafter, the r3PG was initialized from seedling such that the start and end date of the volume simulation (end of rotation age) for each compartment was equivalent to the age at the time the stand volumes were captured in the field. The simulated or modelled volumes and age for each compartment were then compared to compare the modelled versus the observed results (**Figure 4.6**).

### 3.4.2 Actual weather data for model testing

The weather data used to test the 3PG model in this study was obtained from a parallel detailed study by Gakenou (2021). In that study, observed long-term daily weather data including maximum temperature, minimum temperature, precipitation, and solar radiation were obtained from the South African Sugarcane Research Institute (SASRI) and the South African Weather Services (SAWS) from January 2008 to September 2018, corresponding to the period within which field forest inventories were carried out. These data were necessary for testing the r3PG model parameters with ground data prior to use over the study area. Gakenou (2021) used a total of 155 weather stations from the SASRI and SAWS databases to create detailed surfaces of monthly temperature and precipitation using the Random Forest (RF) algorithm. The estimates of “actual” weather data at the reference sites were extracted for each month during the period 2008 – 2018. RF have been widely used to spatially interpolate weather and climate data (Appelhans *et al.*, 2015; Belgiu and Drăgu, 2016; Sekulić *et al.*, 2020, 2021). For RF modelling, the

`randomForest` package (Liaw and Wiener, 2002) in statistical package R (R Core Team, 2021) was used.

**Table 3.4** Sites used to verify the performance of the r3PG model prior to use for future projections.

Company	Compartment name	Latitude	Longitude	Elevation (m)	Spacing (m x m)	Plot area (ha)	Soil form
Sappi	Futululu E6a	-28.39	32.22	53	3.0 x 2.2	0.0514	Fw
Sappi	Mavuya B3a	-28.54	32.20	39	3.0 x 2.2	0.0508	Fw
Mondi Forest	Mtubatuba B003	-28.42	32.21	4.5	2.5 x 3.0	0.0479	Fw1210
Mondi Forest	Nseleni J006	-28.68	32.04	43	2.5 x 3.0	0.0433	Hu2200
Mondi Forest	Nyalazi B032	-28.21	32.33	29	2.5 x 3.0	0.0483	Cv21
Sappi	PalmRidge C15a	-28.34	32.24	59	3.0 x 2.2	0.0515	Fw
Sappi	Salpine F7	-28.56	32.21	54	3.0 x 2.2	0.0535	Fw
Sappi	Salpine G22b	-28.54	32.23	20	2.7 x 2.2	0.0594	Fw
Sappi	Salpine G33b	-28.54	32.23	20	3.0 x 2.2	0.0660	Fw
Mondi Forest	Siyaqhubeka A017	-28.68	32.14	32	2.5 x 3.0	0.0491	Vf2110
Mondi Forest	Siyaqhubeka B044	-28.97	31.64	55	2.5 x 3.0	0.0500	Hu2100
Mondi Forest	Siyaqhubeka F011A	-28.62	32.18	63	2.5 x 3.0	0.0488	Ct2100
Sappi	SouthAreas B35b	-28.68	32.09	60	3.0 x 2.2	0.0535	Fw
Sappi	Terranera B38	-28.67	32.10	62	3.0 x 2.2	0.0535	Fw
Sappi	Terranera C55	-28.70	32.08	41	3.0 x 2.2	0.0535	Fw
Sappi	Trust D13b	-28.51	32.12	63	3.0 x 2.2	0.0660	Fw
Sappi	Trust E23f	-28.52	32.15	44	3.0 x 2.2	0.0660	Fw
Sappi	Trust E24g	-28.53	32.15	44	2.7 x 2.4	0.0648	Fw

### 3.4.3 Soils data for model testing

The soil data and available soil waters (minimum, initial and maximum) that were used in this study to test the applicability of the 3PG model and parameters were results from detailed studies by Gakenou (2021) and Sibiyi (2021). Besides weather, running the r3PG model for the 18 field sites required soil texture information and available soil water as inputs. Sibiyi (2021) collected the soil data from field work in 2018 on the 18 sites. During that study, soil samples were cored at the centre of permanent sample plots (PSP) in the field sites at 10 cm intervals up to a depth of 1.2 m for textural analysis. Using the South African soil texture triangle (Warburton and Schulze, 2006; Schulze, 2007) the textural analyses revealed that the sites were relatively homogeneous sandy soils, except one compartment that was loamy sand (Nyalazi B032). To acquire the soil organic matter to calculate the available soil water, soil samples were cored at three different points 2 m and 90° away from the PSP centre, clockwise from the southwest direction. Samples were collected at 0-10 cm, 10-20 cm, and 20-50 cm depths. In his study, Gakenou (2021) derived the soil's available water capacity (adopted as the initial available soil water,  $asw_i$ ) from the soil texture and organic matter using Saxton and Rawls (2006) soil water characteristics equation.

For this study herein, in r3PG, maximum available soil water was derived as a product of soil depth and initial available soil water, while minimum available soil water was set to zero.

Given the difficulty in reliably estimating the model's "fertility rating" (FR), and because the region is characterized by relatively homogenous soils, FR was set to a constant value of 0.5.

#### **3.4.4 Atmospheric CO<sub>2</sub> concentration**

This study tested the influence of projected rising atmospheric CO<sub>2</sub> concentration on modelled stand volume in r3PG, motivated by the "inconclusivity" in the literature (Section 2.7.1) over the uncertainties associated with the effect of increasing concentration of atmospheric CO<sub>2</sub> on tree growth in the intermediate and long term. The test results are reported in Section (4.3.1).

After the tests, the atmospheric CO<sub>2</sub> was kept constant at 407.1 based on the current scenario (Smith and Wigley, 2006; Clarke *et al.*, 2007; Wise *et al.*, 2009) obtained by averaging the reported values from 2014 to 2021. All the forest yield modelling for all the scenarios was executed with atmospheric CO<sub>2</sub> concentration value.

#### **Other 3PG model assumptions and specifications**

- Parameters for the eucalypt and pine germplasm were constant for all runs using parameters in Table 3
- Planting spacing (3x2m, 1667 trees per hectare) for *E. g x u*
- 1372 trees per hectare for PE
- Fertility rating was set as 0.6
- There were no soil nutrient limitations (including soil exhaustion) considered during the simulations.
- There was no change in soil fertility, available soil water, land uses and changes,
- There were no management interventions such as silvicultural practices, irrigation, and so forth.

Therefore, the stand volumes derived here were only affected by solar radiation, air temperature, photoperiod, atmospheric CO<sub>2</sub>, genotype and plant stocking density and water deficit.

### **3.5 Future climate runs**

The climate data from the WorldClim data had minimum and maximum monthly temperature (*tmin* and *tmax*), mean monthly precipitation (*prec*) and monthly solar radiation *srad* as raster

surfaces. The MAT was calculated by averaging the monthly *tmin* and *tmax* surfaces and the MAP calculated by averaging the using the monthly *prec* surfaces – both using the Raster Calculator tool in ArcGIS version 10.8. the same was done for the *srad* surfaces. Thereafter, all the climate attributes from the different scenarios were extracted to the 5x5 grid points of the study area.

Following testing of the r3PG model's general capability in the region model runs were undertaken using future climate data from the GCMs (Section 1.3 above).

To get a feel for model performance, an initial set of nine runs were conducted in r3PG using future climate data to check if the volume outputs mimicked the pattern of coastal Zululand's known rainfall gradient; increasing MAP from north to south (du Plessis and Zwolinsky, 2003). Thereafter, the model was run for the full set of points for the five different periods: current (1970 – 2000), two intermediate (2041 – 2060 on RCP 4.5 and RCP 8.5), and two future (2081 – 2100 on RCP 4.5 and RCP 8.5).

### 3.6 Site suitability and species choices

Smith *et al.* (2005) summarised the optimum growth criteria of principal commercial forest tree species grown in South Africa and related this information to a forest site classification based on forest economic zone, climate and altitude or climatic, topographic, and edaphic factors (**Figure 3.3**). The optimum growth criteria for the species were described in terms of MAT and MAP. In order to relate optimum growth criteria to altitude, the relationship between altitude range and MAT class was defined for 11 forest economic zones in the summer rainfall regions of South Africa (Smith *et al.*, 2005).

*Pinus elliottii* or *P. elliottii* was an alternative species to *E. g x u* considered for modelling. It was chosen based on the following criteria;

- Site-species matching in Zululand which is a summer rainfall region. Described as having a subtropical climate (ST) (Warburton and Schulze, 2008)
- Availability of 3PG-required species parameters for South Africa –PE have published parameters for South Africa (Sithole, 2011)
- Commercial desirability of species (yield, risk, market) – Of the species; which ones are desired commercially based on yield, risk, and market? What risk factors are considered such as drought sensitivity, pest and disease risk, susceptibility to frost, snowfall, and hail?



In a case where a range of species is suitable for a particular climatic zone (and market), comparative yield determined the preferred species.

Following the site : species matching work done by Smith et al., (2005) (Figure 3.3), the suitability of the study area for the cultivation of *E. gxu* and *P. elliotii* was mapped for the current climate as well as the four future projected scenarios, based on the MAP and MAT of a site. Probable future site classifications were projected for the 5x5km grid points under the four potential future scenarios to establish site class shifts and expected future productivity of those areas during that period. MAT and MAP were used to estimate shifts within the sub-tropical classes in the study area.

Climate zone	Sub-tropical								
	ST1	ST2	ST3	ST4	ST5	ST6	ST7	ST8	ST9
Site class	Frost free								
Frost zone									
Region									
Northern Province	1050 - 0750			0850 - 0600			0500 - 0450		
Gauteng and Free State	N/A			N/A			N/A		
Eastern Mpumalanga	0900 - 0600			0700 - 0450			0450 - 0350		
South eastern Mpumalanga	0900 - 0650			N/A			N/A		
Swaziland	0900 - 0600			N/A			N/A		
Maputaland	N/A			N/A			0100 - 0000		
Zululand and Babanango	0750 - 0450			0550 - 0100			0100 - 0000		
Northern KwaZulu-Natal	0900 - 0650			0650 - 0400			N/A		
KwaZulu-Natal Midlands	0550 - 0300			0300 - 0000			N/A		
Southern KwaZulu-Natal	0500 - 0100			0200 - 0000			N/A		
Eastern Cape	0150 - 0000			N/A			N/A		
MAT (°C)	19 - 20			20 - 21			21 - 22		
MAP (mm)	< 925	925 - 1025	> 1025	< 950	950 - 1050	> 1050	< 975	975 - 1075	> 1075
<i>E. gxu</i>	DR			DR			DR		
<i>E. macarthurii</i>									
<i>E. nitens</i>									
<i>E. nobilis</i>									
<i>E. saligna</i>									
<i>E. smithii</i>									
<i>P. elliotii</i>	DR			DR			DR		

Figure 3.3 Sub-tropical (ST) site classes for commercial plantation species based on ranges of mean annual precipitation and meant annual temperature (Source: Modified from Smith et al., 2005)

### 3.7 *Leptocybe invasa* pest modelling

*Leptocybe invasa*, also known as the blue gum chalcid, is a gall wasp native to Australia in the native range of various host *Eucalyptus* (Nugnes et al., 2015). In South Africa, *L. invasa* was first detected in 2015 and is now present in all the places where *Eucalyptus* is found, including coastal



Zululand (Mphahlele *et al.*, 2021). *Leptocybe invasa*'s small dimensions make it difficult to detect and easy to disperse through unintentional carriage and wind (Otieno *et al.*, 2019). Most detection of heavy infestation in eucalypts is characterised by gall formation on leaves and leaf petioles, midribs and young twigs, which usually results in deformation of the leaf shape (Mphahlele *et al.*, 2021). Heavy infestations can firstly cause leaf deformation, due to curling of the midribs, premature aging and leaf fall (Nugnes *et al.*, 2015), and eventually stunted growth of the tree (Mendel *et al.*, 2004). The preferred climates for *L. invasa* are shown in **Table 3.5**.

Based on *L. invasa*'s favoured conditions (preferred climate and presence of eucalypts), the current and possible future distribution and occurrence of the pest can be modelled. Maxent (Phillips *et al.*, 2004; 2006) is a general purpose niche modelling algorithm for estimating the probability of distributions based on the principle of maximum entropy (Barredo *et al.*, 2015). The model requires a set of environmental predictors and records of presence of the species (Phillips *et al.*, 2004). The machine learning algorithm of Maxent is non-linear, nonparametric, and not sensitive to multicollinearity of the input variables. The presence locations define the constraints on the probability distribution in terms of suitable range of the environmental predictors. The initial assumption is that a species probability of occurrence in the landscape is perfectly uniform and only deviates from this assumption when forced to by the applied constraints. The model output is a probability distribution based on the scores assigned to each pixel and a set of statistical measures of the model's reliability.

In this study, first 19 bioclimatic raster surfaces (**Table 3.6**) were calculated for the present and future climate scenarios in R by stacking the different climate surfaces from the Worldclim data. An R version of the Maxent algorithm built using the **dismo** package (Hijmans *et al.*, 2021) was used. In Maxent, recorded *L. invasa* presence points, raster of *Eucalyptus* forests, and a shapefile of the South African national boundary were loaded. The *L. invasa* presence points were GPS points from field surveys by the ICFR (n.d.). The points were sites where the wasp was detected and the biological control, *Selithricodes neseri*, was released, which were sites with a high infestation of *Leptocybe invasa*. The *Eucalyptus* forests and the 19 bioclimatic variables were used as environmental parameters to define the ecological niche or predictor for *L. invasa* infestation. Maps of present and future potential pest occurrence were produced using the Maxent model (Phillips *et al.*, 2006; Elith *et al.*, 2011).

**Table 3.5** Preferred climate for *Leptocybe invasa* (sourced from CABI, 2021<sup>15</sup>)

Climate	Status	Description
<b>Tropical rainforest climate</b>	Preferred	> 60mm precipitation per month
<b>Tropical monsoon climate</b>	Preferred	Tropical monsoon climate (< 60mm precipitation driest month but > (100 - [total annual precipitation(mm)/25]))
<b>Tropical savanna climate with dry summer</b>	Preferred	< 60mm precipitation driest month (in summer) and < (100 - [total annual precipitation{mm}/25])
<b>Tropical wet and dry savanna climate</b>	Preferred	< 60mm precipitation driest month (in winter) and < (100 - [total annual precipitation{mm}/25])
<b>Steppe climate</b>	Preferred	> 430mm and < 860mm annual precipitation
<b>Desert climate</b>	Preferred	< 430mm annual precipitation
<b>Warm temperate climate with dry summer</b>	Preferred	Warm average temp. > 10°C, Cold average temp. > 0°C, dry summers
<b>Warm temperate climate with dry winter</b>	Preferred	Warm temperate climate with dry winter (Warm average temp. > 10°C, Cold average temp. > 0°C, dry winters)
<b>Warm temperate climate, wet all year</b>	Preferred	Warm average temp. > 10°C, Cold average temp. > 0°C, wet all year

**Table 3.6** Bioclimatic variables used in Maxent to calculate *Leptocybe invasa* risk

Variable	Description
<i>Bio1</i>	Annual mean temperature
<i>Bio2</i>	Mean Diurnal Range (Mean of monthly (max temp - min temp))
<i>Bio3</i>	Isothermality (BIO2/BIO7) (* 100)
<i>Bio4</i>	Temperature Seasonality (standard deviation *100)
<i>Bio5</i>	Max Temperature of Warmest Month
<i>Bio6</i>	Min Temperature of Coldest Month
<i>Bio7</i>	Temperature Annual Range (BIO5-BIO6)
<i>Bio8</i>	Mean Temperature of Wettest Quarter
<i>Bio9</i>	Mean Temperature of Driest Quarter
<i>Bio10</i>	Mean Temperature of Warmest Quarter
<i>Bio11</i>	Mean Temperature of Coldest Quarter
<i>Bio12</i>	Annual precipitation
<i>Bio13</i>	Precipitation of Wettest Month
<i>Bio14</i>	Precipitation of Driest Month
<i>Bio15</i>	Precipitation Seasonality (Coefficient of Variation)
<i>Bio16</i>	Precipitation of Wettest Quarter
<i>Bio17</i>	Precipitation of Driest Quarter
<i>Bio18</i>	Precipitation of Warmest Quarter
<i>Bio19</i>	Precipitation of Coldest Quarter

<sup>15</sup> <https://www.cabi.org/isc/datasheet/108923>

## Chapter 4 Results

### 4.1 Climate

#### 4.1.1 Temperature



**Figure 4.1** Projected mean annual temperature change under RCP 4.5 at each 5x5 grid point. The blue plus sign (+) represents current temperature (1970 – 2000), the green circle (o) intermediate temperature (2041 – 2060), and the red triangle (Δ) future temperature (2081 – 2100).

In **Figure 4.1** above, all the grid points in the site showed projected increases in MAT from their current (1970 – 2000) values along RCP 4.5. MAT increments ranged from 0.6 – 2.1°C from the current to the intermediate range (2041 – 2060) and from 1.4 - 2.9°C for the future range (2081 – 2100). The same was true for MAT change in RCP 8.5. The points exhibited projected MAT increases from the current to the intermediate scenario (1.0 – 2.5°C) as well as to the future scenario (3.2 – 4.6°C).

The most notable difference between the two pathways is the rate of increase of MAP which can be observed by comparing the spaces between point distributions in **Figure 4.1** and **Figure 4.2**. In **Figure 4.1**, the space between the blue pluses (representing the current scenario) and the green circles is larger than the space between the green circles and the red triangles (future scenario). This shows a greater increase from the current to the intermediate scenario than from the intermediate to future. This mimics the radiative forcing of RCP 4.5 in which emissions are imagined to start declining by 2045 (Collins *et al.*, 2013). **Figure 4.2** shows the consecutive spaces increasing therefore reflecting the “business as usual” scenario of RCP 8.5 in which emissions continue to rise throughout the 21<sup>st</sup> century (Collins *et al.*, 2013; Tadross *et al.*, 2017).

The projected ranges of MAT increase are consistent with some of the literature. For instance, Engelbrecht (2019) used a CCAM downscaling of six GCMs from the CMIP5 experiment to predict MAT over South Africa. Engelbrecht (2019) found that under a low mitigation scenario (RCP 8.5) MAT for coastal Zululand could rise up to 1 - 2°C for the period 2021 – 2050 and 3 - 4°C for the period 2070 – 2099. The ambitious mitigation scenario RCP 4.5 could see increases of between 0.5 - 2°C and up to 1 – 2.5°C for the intermediate and future periods respectively (see also Engelbrecht *et al.*, 2015; Tadross *et al.*, 2017).

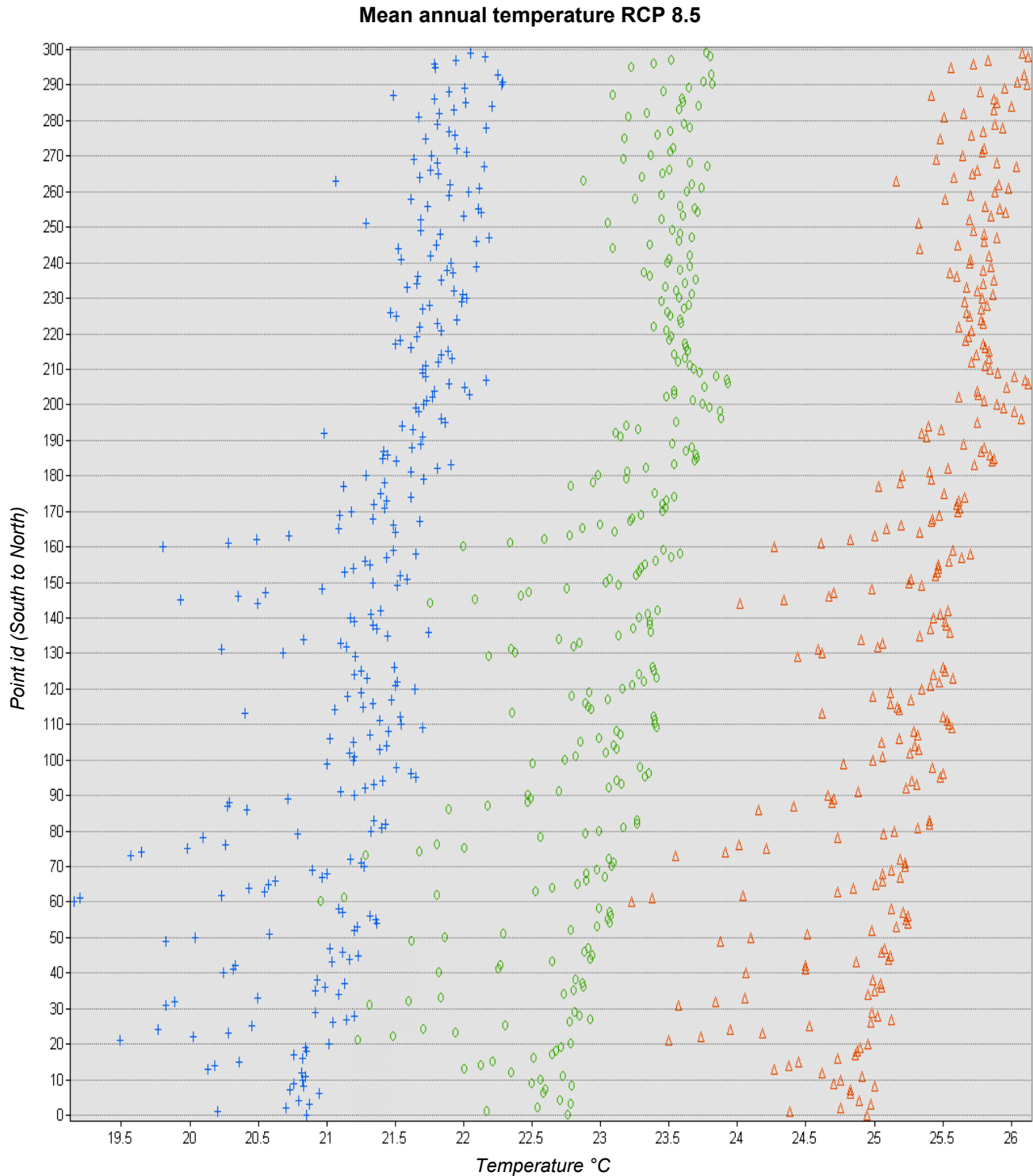


**Figure 4.2** Projected mean annual temperature change under RCP 8.5 at each 5x5 grid point. The blue plus sign (+) represents current temperature (1970 – 2000), the green circle (o) intermediate temperature (2041 – 2060), and the red triangle (Δ) future temperature

### 4.1.2 Precipitation

For both projected periods, a decrease in mean annual precipitation (MAP) was predicted from the South towards the North and from the East, along the coast of Zululand, and inland towards the West. The trend in precipitation change is consistent with what was predicted in other studies (see Warburton and Schulze, 2008). There was, however, a smaller reduction in precipitation between 2000 - 2041 than between 2000 - 2081 (**Figure 4.3**). In the study area, the north to mid latitudes experienced a greater loss in precipitation as compared to the areas in more southern latitudes. In fact, in both the intermediate and long-term future scenario for RCP 4.5, some areas in the southern latitudes showed an increase in precipitation from the year 2000. Under the ambitious RCP 4.5, approximately 73% of the points/region decreased in rainfall from the current to the intermediate period (2000 - 2041) and this increased to 90% in the future period (2000 - 2081).

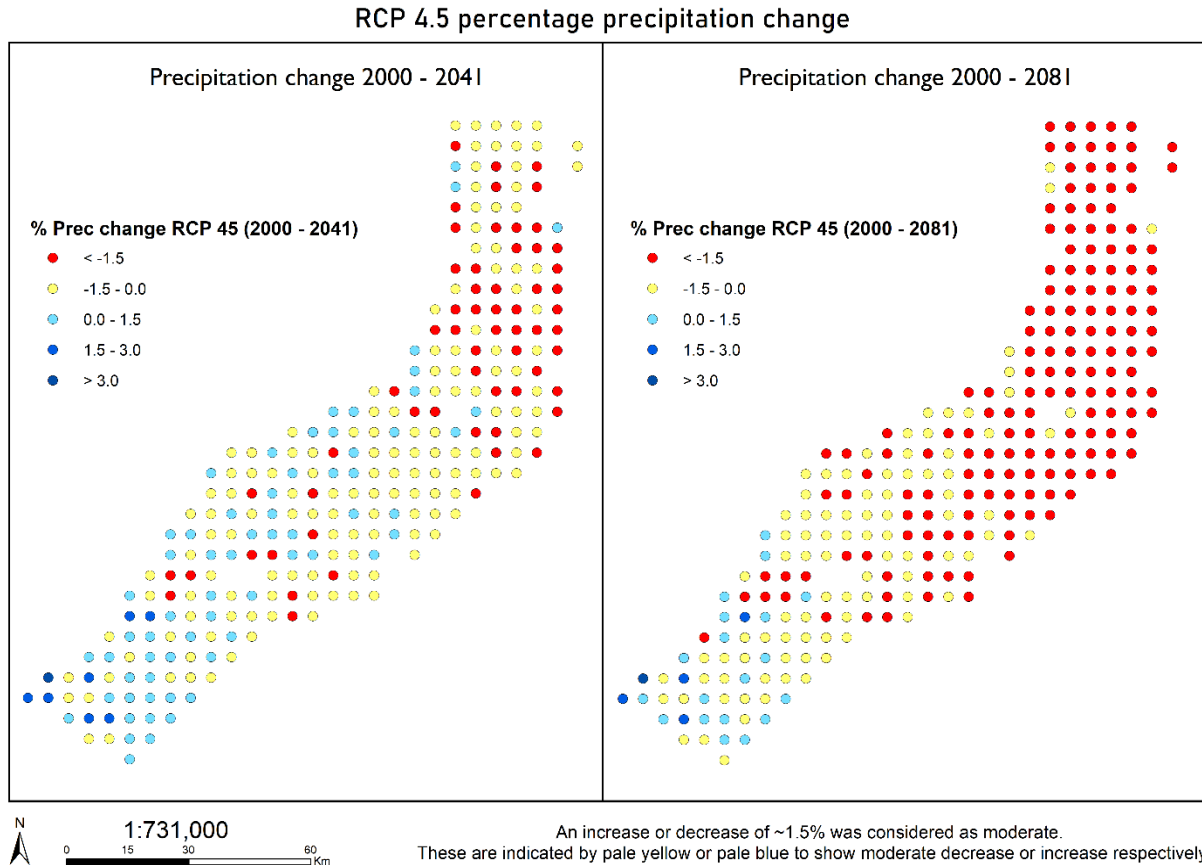


**Figure 4.3** Change in precipitation from the year 2000 to 2041 (left) and to 2081 (right) for RCP 4.5. The precipitation change is shown on a colour scale from red, representing the biggest loss, to navy blue representing a gain in precipitation

**Table 4.1** Shifts in the percentage of the area that loses precipitation in RCPs 4.5 and 8.5.

	RCP 4.5		RCP 8.5	
	Current to 2041	Current to 2081	Current to 2041	Current to 2081
% of points with decrease	72.8	90.2	14.5	40.2
% of points with increase	26.1	8.7	84.4	59.4
% no change	1.1	1.1	1.1	0.4

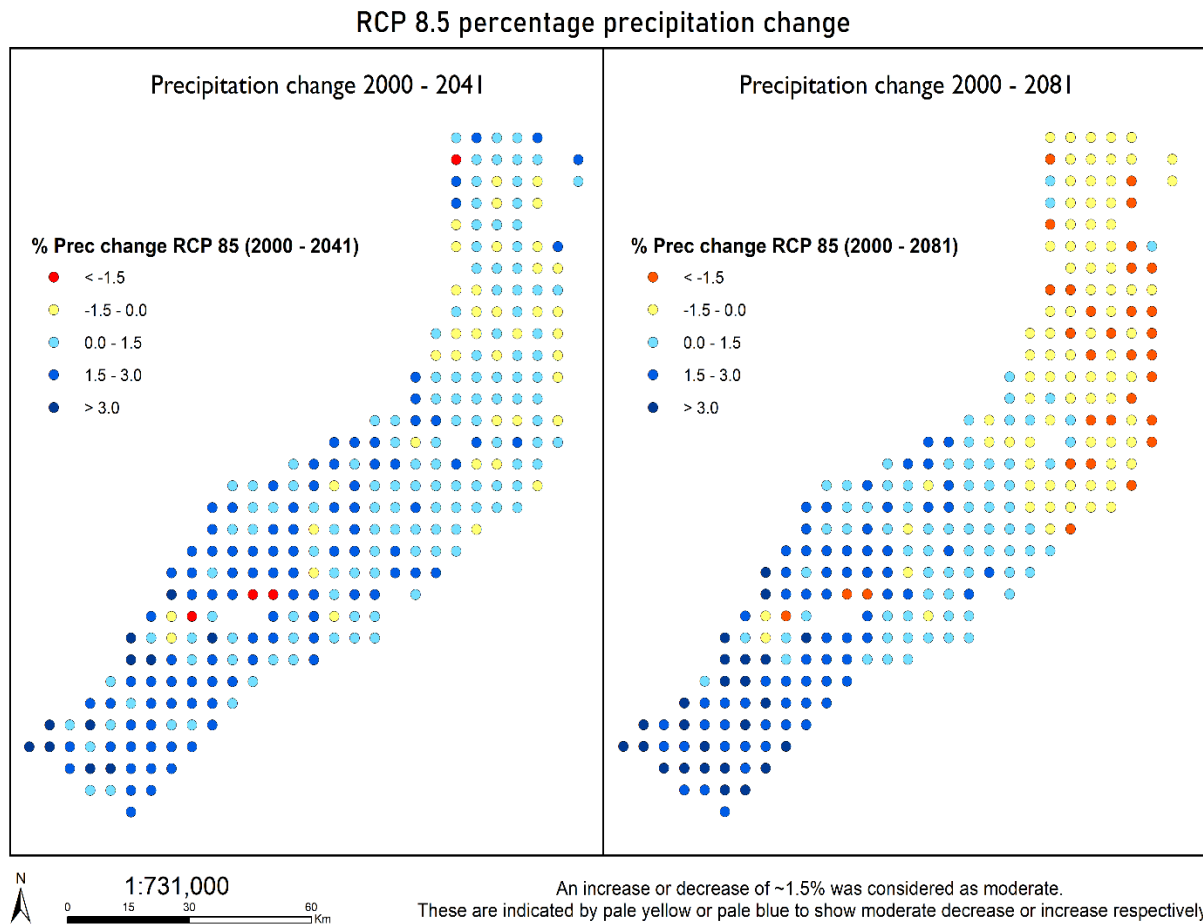


**Figure 4.4** Change in precipitation from the year 2000 to 2041 (left) and to 2081 (right) from the WorldClim data for RCP 8.5. The precipitation gain change is shown on a colour scale from red, representing the biggest loss, to navy blue representing a gain in precipitation.

The scenarios in RCP 8.5 also showed a general trend similar to RCP 4.5 (**Figure 4.3** and **Figure 4.4**) with a reduction in MAP in the north from the year 2000. However, this projected reduction was markedly less and most areas in the mid to southern latitudes, both in the change

from 2000 - 2041 and 2000 - 2081, showed greater increases in MAP along RCP 8.5 as compared to what was observed in RCP 4.5. The period from intermediate period (2000 – 2041) in RCP 8.5 projected an increase in MAP in 84% (against 26% in RCP 4.5 in the same period) of the points/region which then reduced to 59% (compared to 9% in RCP 4.5) for the future period (2000 – 2081) (**Table 4.1**).

Some studies and climate experiments have found comparable results in projecting future precipitation over coastal Zululand. Under RCP 8.5 for the intermediate period 2021 – 2050, Engelbrecht (2019) projected an increase in rainfall over the Zululand coast while the north-eastern parts of South Africa were projected to become drier. On the other hand, while rainfall is projected to decrease over most of coastal Zululand for 2070-2099 under RCP 4.5, some parts are projected to experience increased rainfall (Tadross *et al.*, 2017; Engelbrecht, 2019).

## 4.2 Future shifts in site species suitability

Using the site classification system summarized in **Figure 3.3** (Smith *et al.*, 2005), for RCP 4.5, most sites shifted from ST3 and ST5 – ST7 to ST8 or ST9 (**Figure 4.5** top left). The northernmost latitudes maintained their current classification ST7 (MAT = 21 – 22 °C and MAP < 975 mm) which is considered a drought risk (DR) (Smith *et al.*, 2005). By 2100 along RCP 4.5, it was projected that most sites in the mid to southern latitudes would have shifted to ST8, whilst the points over the existing plantations and close to the coast of Zululand would maintain ST9. Similarly, along RCP 8.5, while the northernmost latitudes maintained their site class ST7, most of the classes were projected to shift to ST8 by 2100 and the points along the coast of Zululand in our study area would maintain their ST9 status. **Table 4.2** shows the percentage of points belonging to a particular site class per scenario and the shifts along each RCP.

**Table 4.2** The projected percentage of points belonging to site classes per scenario

Site class	Percentage of points in site class				
	Current	RCP 4.5		RCP 8.5	
		2041 - 2060	2081 - 2100	2041 - 2060	2081 - 2100
ST3	4.3	0.0	0.0	0.0	0.0
ST5	5.8	0.4	0.0	0.0	0.0
ST6	12.3	0.7	0.0	0.0	0.0
ST7	9.8	11.2	10.1	12.0	10.1
ST8	22.8	36.2	22.8	44.9	22.8
ST9	44.9	51.4	67.0	43.1	67.0



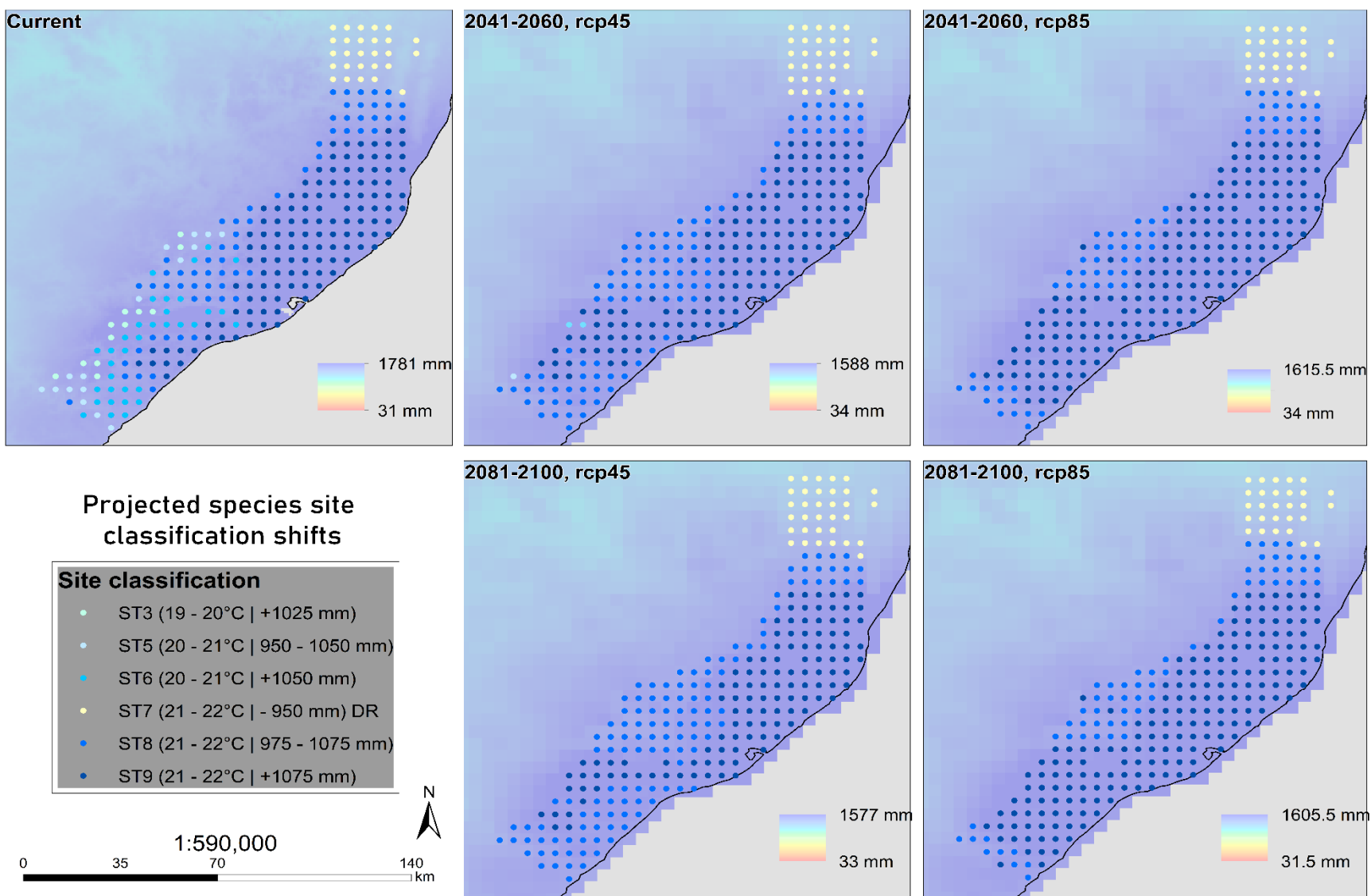


**Figure 4.5** The projected site classification shifts for the study region over projected precipitation for the respective scenario.

### 4.3 Testing and validating of the r3PG model

The predicted r3PG volume was compared against the field collected (observed) volume in the 18 ground sites in **Figure 4.6**. The results of the comparison are further given in **Table 4.3**, in which we obtained a significant  $R^2$  value of 0.88 and p-values of 0.07 for the intercept and  $1.17E-08$  for the coefficient of the observed volume. These results determined the application of the r3PG model parameters to the study grid points.

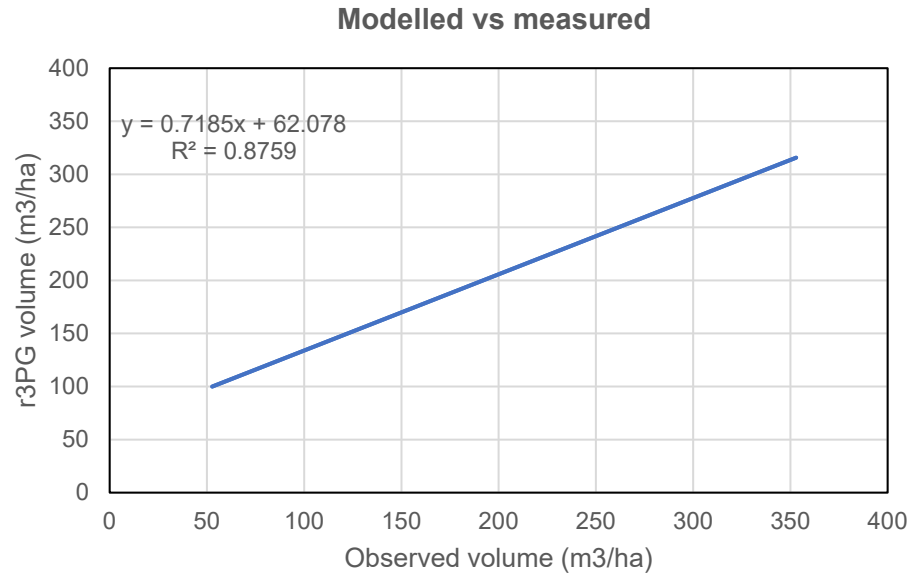


**Figure 4.6:** Plot of r3PG modelled volume against field observed volume in the 18 test sites.

**Table 4.3** Summary statistics of the plot of modelled versus observed volume

<b>Regression Statistics</b>	
Multiple R	0.93588101
R Square	0.87587327
Adjusted R Square	0.86811535
Standard Error	34.0425587
Observations	18

<b>ANOVA</b>					
	<i>df</i>	<i>SS</i>	<i>MS</i>	<i>F</i>	<i>Significance F</i>
Regression	1	130839.9395	130839.9	112.9005	1.17338E-08
Residual	16	18542.33283	1158.896		
Total	17	149382.2724			

	<i>Coefficients</i>	<i>Standard Error</i>	<i>t Stat</i>	<i>P-value</i>
Intercept	-49.726654	25.64422642	-1.9391	0.070333
3pg_volume	1.21907755	0.114731682	10.62547	1.17E-08

#### 4.3.1 r3PG modelling and increasing atmospheric CO<sub>2</sub> concentration

During this study, after validating the r3PG model with the 18 ground sites, several iterations of the growth modelling showed an increase in stand volume with increasing atmospheric CO<sub>2</sub> concentration even when other important factors such as MAP reduced. **Table 4.4** shows how the highest volume (averaged over all the sites), 441 m<sup>3</sup>ha<sup>-1</sup>, was projected in the future extreme of the low mitigation scenario RCP 8.5, which also had the highest atmospheric CO<sub>2</sub> concentration<sup>16</sup> of 797 parts per million (ppm) (Riahi *et al.*, 2007; Tebaldi *et al.*, 2021). The model did not penalise the stand volume and other processes for increase in CO<sub>2</sub> against unfavourable temperature and precipitation.

**Table 4.4** Changes in average values of stand volume from one of the changing CO<sub>2</sub> test runs with average MAP, MAT and CO<sub>2</sub> across all scenarios

	<b>current</b>	<b>RCP 4.5</b>		<b>RCP 8.5</b>	
		<b>2041 - 2060</b>	<b>2081 - 2100</b>	<b>2041 - 2060</b>	<b>2081 - 2100</b>
<i>Avg CO<sub>2</sub> (ppm)</i>	407	472	532	511	797
<i>Avg MAP (mm)</i>	1082	1078	1067	1097	1092
<i>Avg MAT (°C)</i>	21	23	24	23	25
<i>Avg yield (m<sup>3</sup>ha<sup>-1</sup>)</i>	301	341	365	362	441

Avg = average | ppm = parts per million

#### 4.4 Volume yield

The general projected change in stand volume relative to the current scenario was a decrease in *E. g x u* stand volume along both RCP 4.5 and 8.5 (**Figure 4.7**). However, the rate of volume reduction in terms of the number of points losing volume and the quantity of that volume differed between the two RCPs from the current scenario. Under RCP4.5 there was an average loss of 0.4% of volume from 47.6% of the points from 2000 – 2041, which increased to a loss of 5.1%

<sup>16</sup> CO<sub>2</sub> data accessed from <https://tntcat.iiasa.ac.at/RcpDb/dsd?Action=htmlpage&page=spatial>

from 73.8% of the points from 2000 – 2081. Along the low mitigation pathway RCP 8.5, 47.3% of the points lost an average of 0.1% of volume from 2000 – 2041 which shot up to an average loss of 13.6% from 96.7% of the points by the end of the century (**Table 4.5**).

For *Pinus elliottii*, there was a similar trend for future projections as to the *E. g x u* runs (**Figure 4.8**). There was a general reduction in stand volume yield for pine from the Current scenario to 2100 along both RCP 4.5 and RCP 8.5. Furthermore, the percentage of points that lost volume (corresponding to the size of the region) and the average percentage volume lost (corresponding to total volume lost) was more in RCP 8.5 than it was along RCP 4.5. As shown in **Table 4.5**, it was projected that there could be a 7.3% volume loss from about 67% of the region from the current scenario to 2041. This could increase to a total average loss in volume of 14.6% from 93% of the study area by 2100 in the ambitious scenario RCP 4.5. Adversely, RCP 8.5 was projected to undergo a 7.9% volume loss from 71% of the region by 2041 which could become a 30% volume loss from all the points by 2100.

**Table 4.5** Percentages of number of points that lost volume and the percentage of total average volume lost by those points for both *E. g x u* and *P. elliottii* across all scenarios from the current.

from 2000 to		RCP 4.5		RCP 8.5	
		2041 - 2060	2081 - 2100	2041 - 2060	2081 - 2100
<b><i>E. g x u</i></b>	<i>Average % vol loss</i>	0.4	5.6	0.1	13.6
	<i>% of points that lost vol</i>	47.6	73.8	47.3	96.7
<b><i>P. elliottii</i></b>	<i>Average % vol loss</i>	7.3	14.6	7.9	29.5
	<i>% of points that lost vol</i>	67.6	92.7	70.5	100.0

Common to both *P. elliottii* and *E. g x u* was that the northernmost latitudes appeared to lose more than the rest of the region. Also, for both, over time the regions further from the coast moving inland from East to West appeared to be less likely to show significant future volume reductions than the regions closer to the coast. However, the overall yield and consequently the rate of loss of stand volume was more in *P. elliottii* than it was in *E. g x u* (**Table 4.5**).

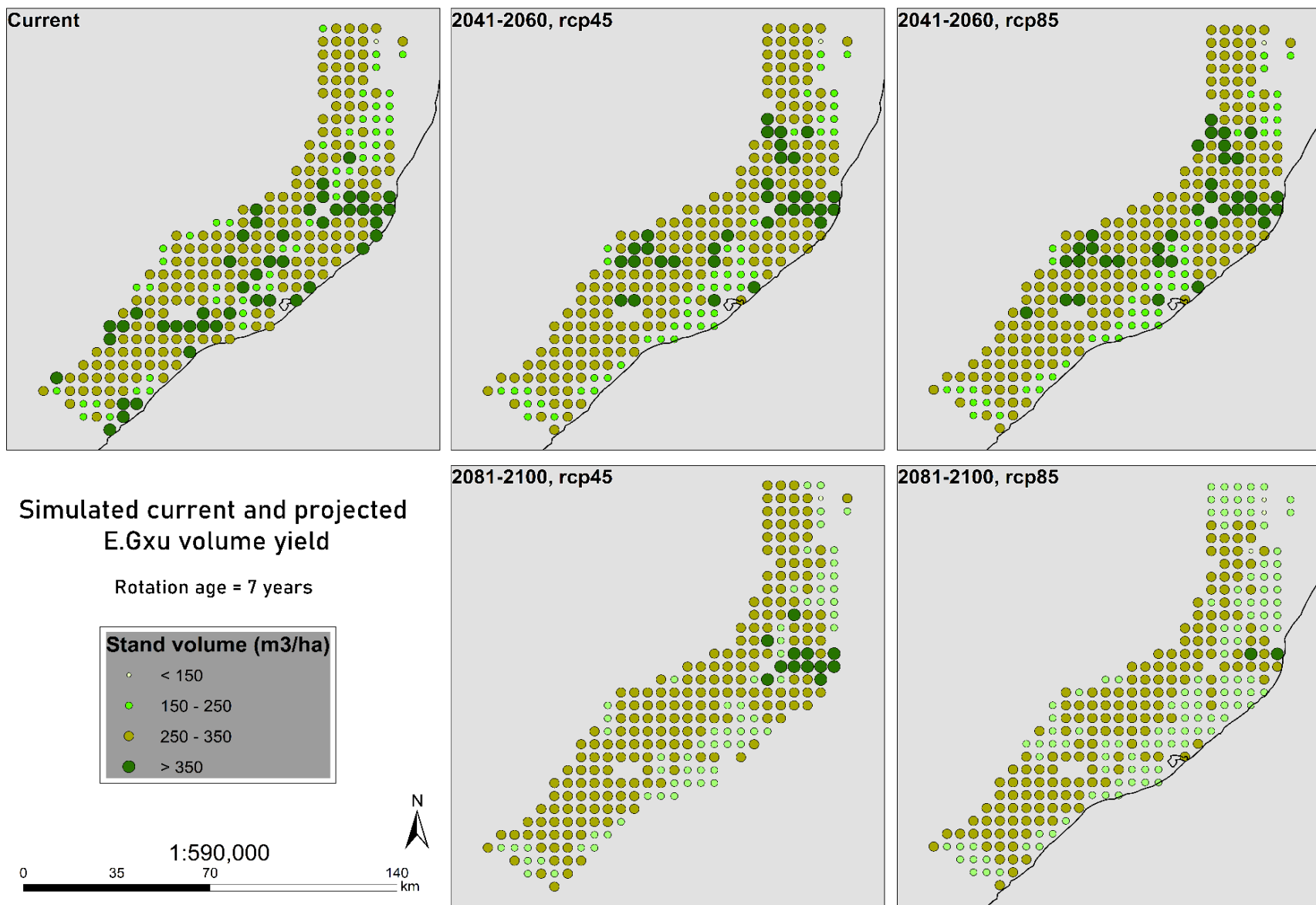


**Figure 4.7:** Modelled current and projected *Eucalyptus grandis x urophylla* stand volume at the end of a 7-year rotation on the 5x5 grid points.

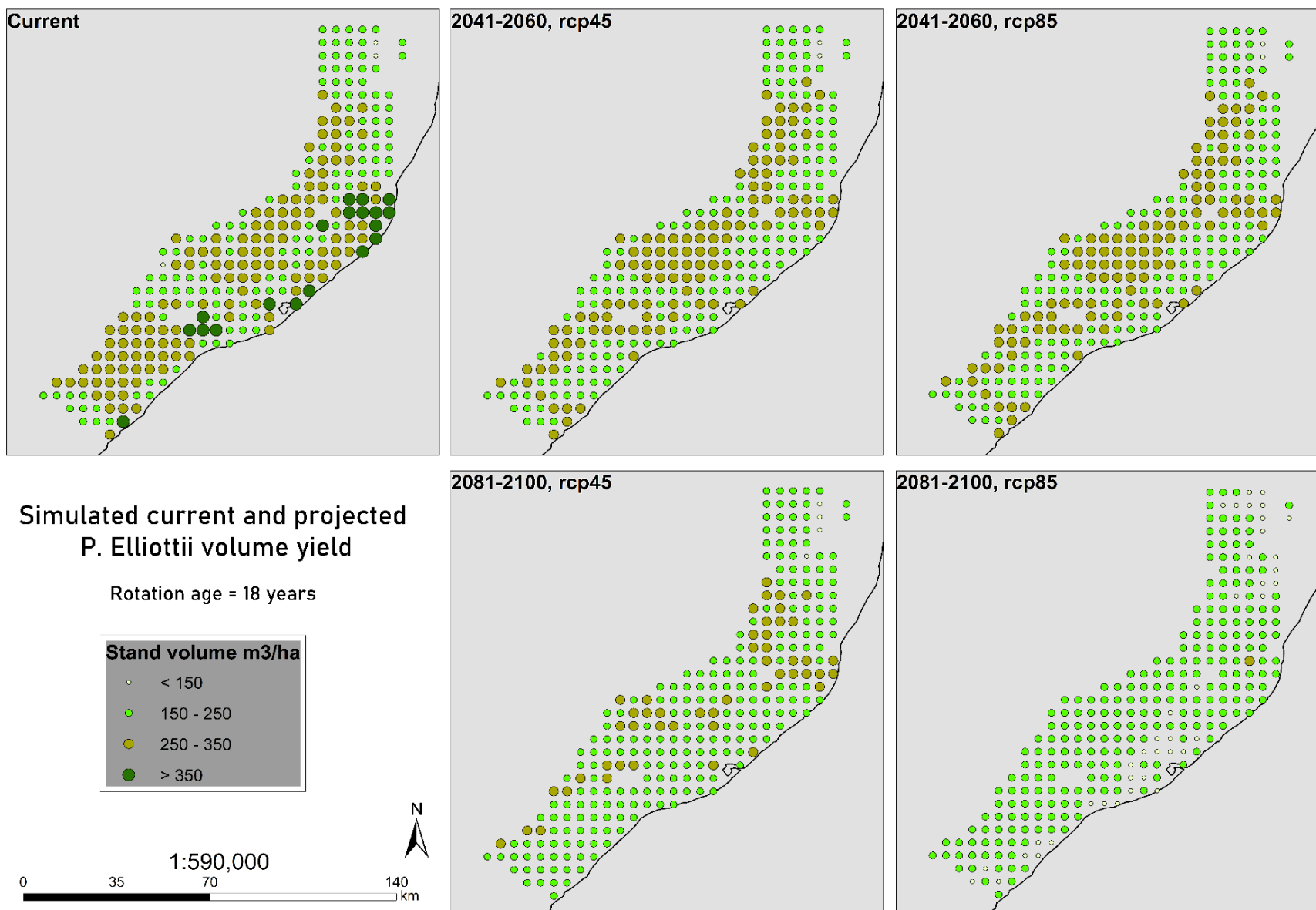


Figure 4.8: Modelled current and projected *Pinus elliottii* stand volume at the end of an 18-year rotation on the 5x5 grid points.

#### 4.5 *Leptocybe invasa* occurrence and risk

Favourable environmental conditions for the occurrence of *L. invasa* reduced in areal extent from the year 2041 to 2100 along both RCPs 4.5 and 8.5 over eastern South Africa (**Figure 4.9**). The decline in coverage or distribution was more dramatic for RCP 8.5 than it was in RCP 4.5. Going inland from east to west also saw a reduction in the extent of the favourable conditions for pest occurrence. Over eastern South Africa areas exposed to a high risk (dark red) increased from 2041 to 2100 along RCP 4.5 while that intensity reduced in RCP 8.5 for the same time period.

Looking closer at the study site in **Figure 4.10**, along RCP 4.5 from 2000 – 2041 there was a rise in the number of sites with a high risk (>70%) of *L. invasa* infestation. Then from 2041 to 2081 the number of areas with a high probability of infestation reduced. According to **Table 4.6** the current scenario had 52.6% of the points in our site projected to have an infestation risk of  $\geq 70\%$ . From the current scenario along RCP 4.5 in the period 2041 - 2060 the number of points projected to have an infestation of  $\geq 70\%$  increased to 86.1% while the remaining 13.9% could have *L. invasa* risk of less than 70%. However, the percentage of high-risk infestation was projected to reduce to 54.4% by 2100, with 34.3% and 11.3% of the study area projected to have risks of < 70% and < 30% respectively.

By 2060 under the low mitigation scenario (RCP 8.5), 79.2% of the site was projected to have highly favourable environmental conditions for *L. invasa* infestation that make an infestation very probable, which was less than the number of projected points under RCP 4.5 (86.1%) for that same time period. The difference was even greater between RCPs 8.5 and 4.5 at the long-term scenario (2081 – 2100) – RCP 8.5 was projected to have 4.4% of the site with a high infestation risk ( $\geq 70\%$ ) while the RCP 4.5 pathway could have 54.4% of at that high risk.

Generally, the mid to southern latitudes were projected to have higher probability of pest presence than the northern latitudes at the end of the century under both RCPs (**Figure 4.10**). The percentage of the site at high risk in the intermediate period (2041 – 2060) in both RCP 4.5 and 8.5 increased from the current – to 86.1% and 79.2% respectively – and then reduced to 54.4% (RCP 4.5) and 4.4% (RCP 8.5) by 2100.

**Table 4.6** Percentage of points distributed by percentage of projected *Leptocybe invasa* risk across all scenarios

		<i>L</i> < 30%	30 ≤ <i>L</i> < 70%	<i>L</i> ≥ 70%
<b>RCP 4.5</b>	Current	1.5	46.0	52.6
	2041 - 2060	0.4	13.5	86.1
	2081 - 2100	11.3	34.3	54.4
<b>RCP 8.5</b>	2041 - 2060	0.7	20.1	79.2
	2081 - 2100	73.0	22.6	4.4

*L* = Risk of *Leptocybe invasa* infestation

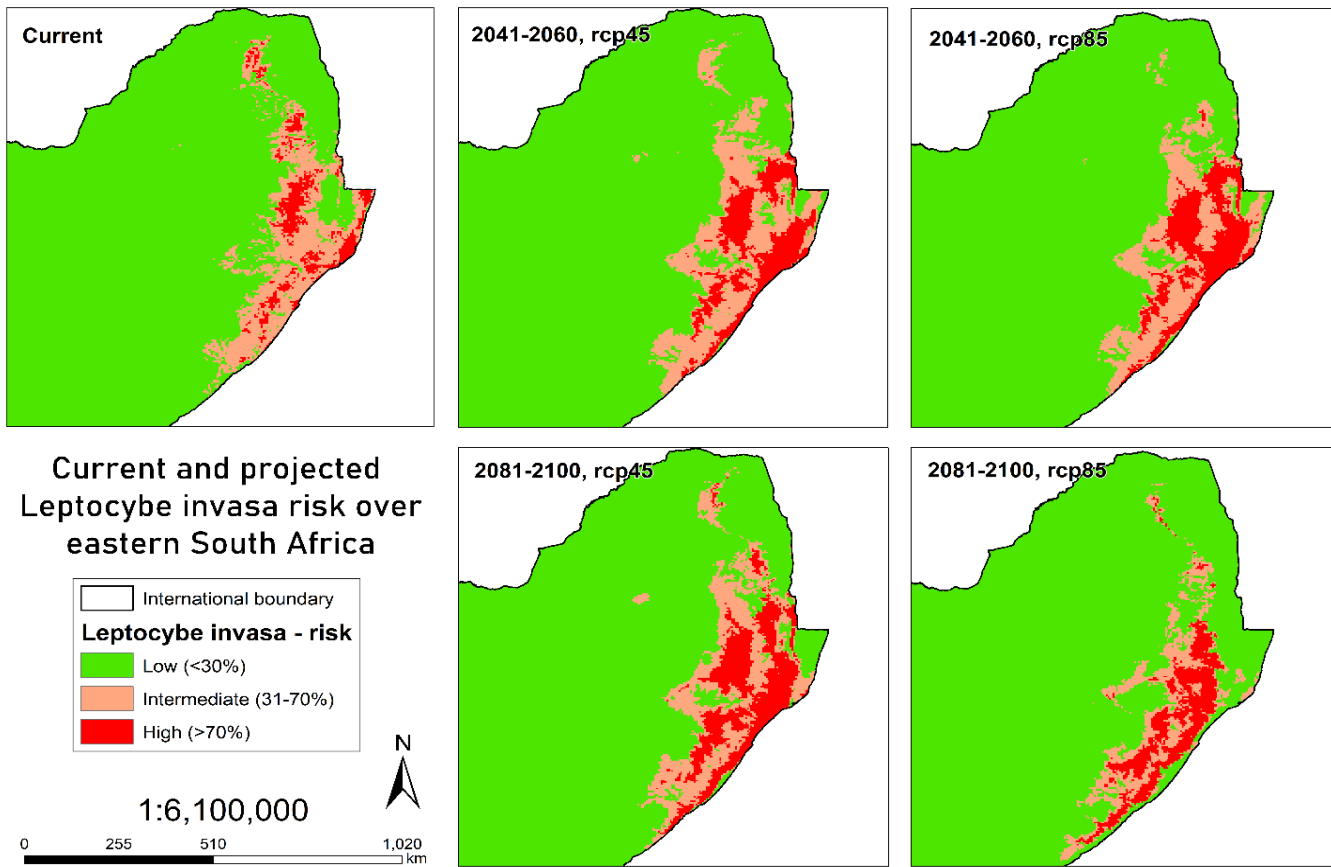


**Figure 4.9** Current and projected probability of *Leptocybe invasa* infestation over eastern and north eastern South Africa



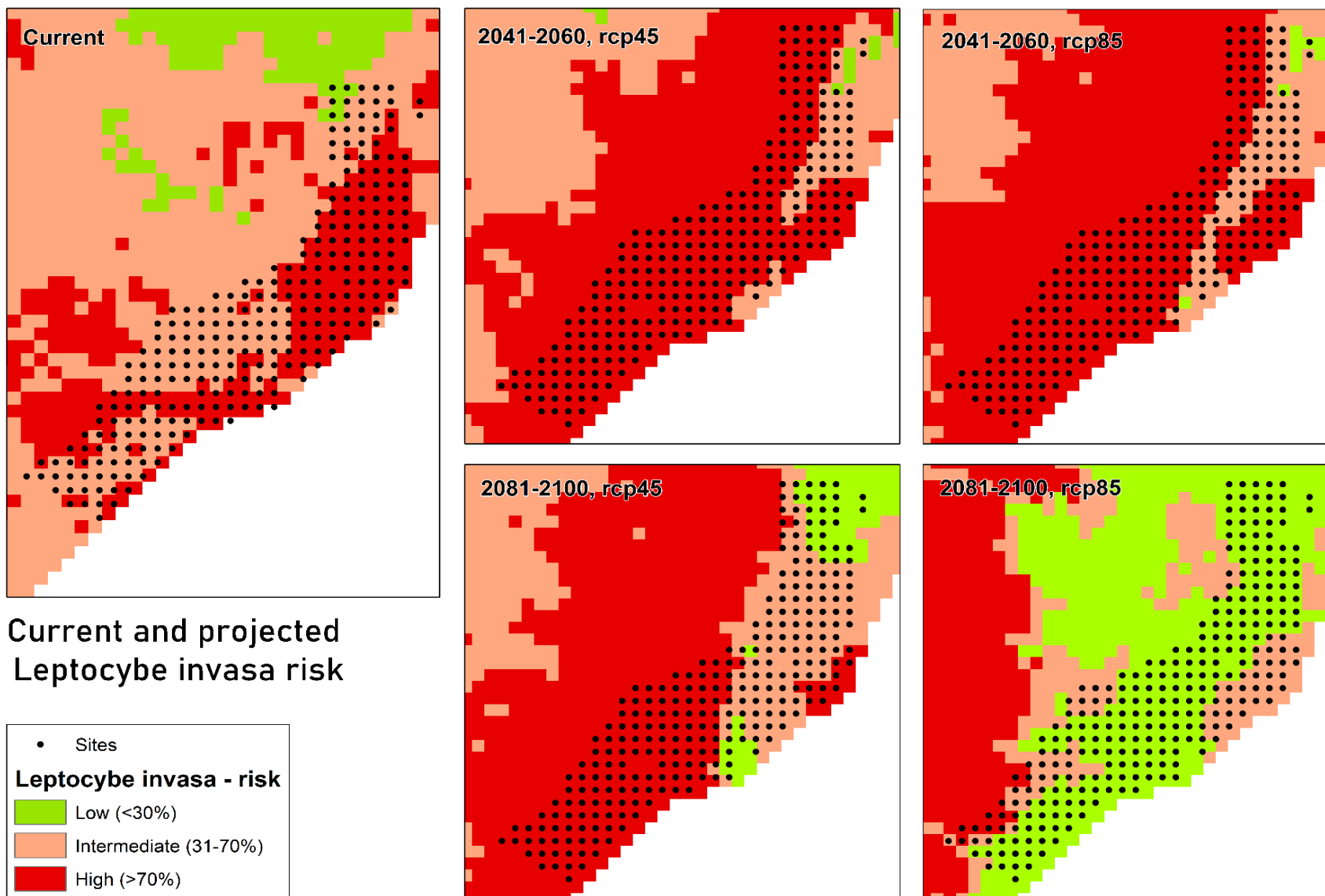


Figure 4.10 Current and projected probability of *Leptocybe invasa* infestation over the study site

## Chapter 5 Discussion and conclusion

The focus of the study was to explore the likely trends and patterns of change in plantation fibre production (stand volume) and pest risk for the important Zululand region of Kwa-Zulu/Natal, South Africa. In an ideal world, the study and the models and the software used herein should have produced exact values of all the intended current and projected variables. But the limitations and uncertainties that come with the use of third-party data and simplified models of real-world phenomena (climate and tree growth) make perfect, absolute predictions impossible. Therefore, the results reported here were of interest to observe projected estimated changes in mean annual temperature, mean annual precipitation, site classification, stand volume and the probability of pest occurrence.

### 5.1 Global circulation models and climate projections

Global circulation models (GCMs) have been criticized for their relatively large uncertainties stemming from imperfect simulation of real-world processes at multiple levels, including biogeochemical processes (Lupo and Kininmonth, 2013), failure to accurately capture important elements of the climate system (e.g., clouds and pressure) (Power *et al.*, 2017), aggregating extreme events and their coarse resolution (Demory *et al.*, 2020). In the context of this study, another important factor which these projections cannot capture is the effect of climate extremes such as periodic droughts, heat waves or flood events, which provoke unique and significant physiological changes in tree growth (Camarero *et al.*, 2018; De Micco *et al.*, 2019). Such events will not be captured by the 3PG model when run on long-term data such as those available from GCMs, as the data do not include them. Nonetheless, the general trend of reduction in precipitation and increase in temperatures is a step closer to more difficult parameters to predict like rainfall variability.

The climate results showed a general projected reduction in the quantity of mean annual precipitation (MAP) over the study area, with some southern latitudes receiving an increase. According to the IPCC (2014) fifth assessment report (AR5) and other studies (Davis-Reddy and Vincent, 2017; Warburton and Schulze, 2008; Xulu *et al.*, 2018) MAP increase and decrease in the region will be accompanied by an increase in rainfall variability. This means that the period within which precipitation falls will become more erratic often happening within fewer days. That means there will be fewer days with high rainfall and more days without rainfall, therefore increasing surface runoff (Engelbrecht, 2019; Germishuizen and Mzinyane, 2017). Additionally,

the projected increase in mean annual temperature (MAP) across all the sites in all the scenarios, will likely increase the rate and quantity of evapotranspiration.

## 5.2 Shifts in site types

According to the report by Smith et al. (2005), Zululand is categorised as having a subtropical (ST) climate based mainly on the ranges of MAP and MAT in the region. In the report the species site suitability classifications under the subtropical category range from ST1 to ST9. Based on the findings of this study, site classification in the study site ranged from ST3 and ST9, without ST4 (**Figure 4.5**). The categories ST4 and ST7 are marked as drought risk (DR) areas due to the MAP (ST4: < 950 mm; ST7: < 975 mm) range being too low for the MAT (ST4: 20 – 21 °C; ST7: 21 – 22 °C).

For a site to be classified as ST8 or ST9, it first has to have  $MAT \geq 21^{\circ}C$ . The next condition is that the site should have  $MAP \geq 975mm$  AND  $< 1075mm$  to be ST8 or  $MAP \geq 1075$  to be ST9 **Figure 4.5**. All the grid points in our study exhibited projected substantial increases in temperatures (see **Figure 4.1** and **Figure 4.2**) which took most of them beyond the  $21^{\circ}C$  into at least ST8. The projected decreases in rainfall across the scenarios do not create significant changes in MAP to less than the threshold of 975mm. Therefore, the shifting of most of the classes to ST8 or ST9 is largely attributed to increases in MAT (Smith et al., 2005).

The classification system according to Smith et al. (2005, p. 7) shows that ST8 and ST9 are favourable for both *E. g x u* and *P. elliotii*. However, with reference to the projected climates in this study, the classification system may need to be expanded to include potential site MATs above  $22^{\circ}C$  but within the classes' MAP ranges (see Annex 1 and 2). The r3PG model showed reductions in yields despite the ST8 and ST9 class designations. This shows that even though a site is climatically suitable according to the classification system used herein, it does not exactly translate into more yield gains. Therefore, the species site classification may only be an indicator of places where the species may grow but not necessarily the best climatic conditions for maximum yield. The approach presented in this study can be seen as a nuanced approach to determining site species suitability because it includes projected volume yield, considers an alternative commercial tree species and models the environmental conditions for pest occurrence. This study also provides more information that can be used for planning towards how to make a site suitable amid changing climates.

### 5.3 3PG as a tool for predicting volume in eucalypt stands

The 3PG model when run for a set of 18 test sites gave reliable rankings for the sites. There was a slope bias, with higher volume sites somewhat under-predicted by the model. Regardless, the model was able to predict volume within reasonable R-squared and p-values (**Table 4.3**) to allow for replication over a large area, as the focus was on the quantity and direction of change in yield and not explicit accurate values.

In this study, the 3PG model, particularly the R version, proved to be versatile and easily adaptable to other data sources. The use of 3PG in an R environment made it easy to link it to the WorldClim data (which can be downloaded with an R-script) and Schulze et al.'s (2005) soils shapefiles to create one large pipeline with less manual intervention. That being said, one major limitation of the 3PG software are that it considers soil to be a homogenous 'bucket' of sorts i.e., 3PG recognizes the soil as being of one type in depth when soil horizons in reality are highly heterogenous (Schulze, 2007). Soil horizons have a significant effect on the formation and growth of roots as well as the flow and intake of nutrients and water. Another limitation of the 3PG model is that its accuracy assessment is limited. There is a lot of potential for developing methods to assess the submodules, processes, and outputs beyond comparing the final outputs after a rotation age with field measurements. Finally, the fact that 3PG requires and gives out information in monthly time steps makes the preparation of input data a critical part of the simulation process e.g., aggregating daily data into monthly values.

### 5.4 Future volume expectations using 3PG

The r3PG model was run to estimate the stand volume yield at each of the 5x5 grid points ( $n = 276$ ). Even though the r3PG model produces other stand variables such as leaf area index, basal area, stand density, and height (Trotsiuk *et al.*, 2020), volume was our target.

This study sought to project the future stand volume or yield of *Eucalyptus grandis* X *urophylla* (*E. g* x *u*) plantations in coastal Zululand based on projected estimates of MAP, MAT and solar radiation. The combination of increased temperatures along with reduced rainfall will reduce the amount of moisture available or accessible by the tree root systems for plant growth (Germishuizen and Mzinyane, 2017). Warburton and Schulze (2008) already found that *E. g* x *u* is highly sensitive to a combination of changing rainfall accompanied by a temperature increase of at least 2 °C. With the projected climates in this study showing a reduction in rainfall of up to 3% and temperature increases of more 2%, a reduction in volume production is inevitable under these circumstances.

The *Pinus elliottii* trials were meant to investigate the possibility of alternatives to *E. g x u* should the projected site suitability for *E. g x u* cultivation change for the worse. Our studies revealed that even though the climatic conditions for the cultivation of both *E. g x u* and *P. elliottii* deteriorated, the *Eucalyptus* crop would be more resilient and therefore provide more yield overtime than the *P. elliottii*, making eucalypts more suitable for the projected conditions.

But it is important to acknowledge that these results were done with CO<sub>2</sub> fertilization ignored because CO<sub>2</sub> fertilization functions in the r3PG model may have had sources of uncertainties (Elli *et al.*, 2020). For instance, this study simulated stand volume against increasing CO<sub>2</sub>, reducing MAP, and increasing MAT and found that the projected stand volume kept correlating positively with increasing CO<sub>2</sub> (**Table 4.4**). These simulations conform with some free-air CO<sub>2</sub> enrichment (FACE) and chamber-studies findings that under elevated CO<sub>2</sub> most plant species show higher rates of photosynthesis, increased growth and decreased water use (Taub, 2010; Thompson *et al.*, 2017). This contrasted findings by Booth (2013) that revealed that despite increasing atmospheric CO<sub>2</sub> concentrations, high temperatures combined with increasing water deficit may increase *Eucalyptus* drought deaths. Other studies are highlighted in Section 2.7.1. Due to the uncertainty in the effect of atmospheric CO<sub>2</sub> concentrations on plants, this study kept the level constant.

To better calibrate the carbon dioxide function in the 3PG model towards more accurate yield modelling and projection in South Africa, it would be necessary to obtain data from empirical studies (ABARES, 2011) based in forest productive regions. The studies would be both where trees have been grown under artificially increased levels of carbon dioxide and historical long-term multi-rotation ordinary field studies where the atmospheric CO<sub>2</sub> concentrations are recorded with forest inventories. Such experiments for trees have gained traction in the Northern Hemisphere (e.g. U.S. DOE, 2020) and Australia (for example [EucFACE](https://www.westernsydney.edu.au/hie/EucFACE)<sup>17</sup>). However, the studies could be problematic both in the length of time required to run the experiment and the ability to mimic altered carbon dioxide conditions for the duration of the experiment for laboratory-based studies. In addition, the exact interactions among increased levels of atmospheric carbon dioxide, soil fertility and other environmental abiotic and biotic attributes which affect plant CO<sub>2</sub> processes are known areas of complexity (ABARES, 2011). Nevertheless, accurate projection of yield using process-based software could benefit from such experiments and efforts.

---

<sup>17</sup> <https://www.westernsydney.edu.au/hie/EucFACE>

## 5.5 Pest risk

This study spatially and temporally identified and predicted potential *Leptocybe invasa* infestation sites based on favourable environmental conditions. Climatic parameters were used to identify the optimum conditions for the pest's presence based on CMIP5 climate data from WorldClim (Fick and Hijmans, 2017) and presence-only data from the ICFR (n.d.), which were projected along RCPs 4.5 and 8.5. The study projected a reduction in the number of areas with a high risk of *L. invasa* infestation in future scenarios across both RCP 4.5 and 8.5. The lowest amount of risk over the area was projected in the most extreme low mitigation scenario, characterised by mostly species site classes ST8 and ST9, the highest MATs and up to 3% reduction in precipitation. It is in this scenario as well where the least volume yield for *E. g x u* was projected.

The *L. invasa* pest costs the South African forestry industry significant losses (Mphahlele *et al.*, 2021). These losses have been attributed to the difficulty in detecting the pest at early onset, the difficulty in treating and containing the pest invasion, and more importantly the inability to quantify possible forest canopy losses caused by the pest. The *L. invasa* attacks the leaves of eucalypts which reduces photosynthetic potential and biomass allocation within trees (Nguyen *et al.*, 2015).

There are several advantages of Maxent that make it appropriate for estimating the probability of occurrence of pests. To begin with, the output from the Maxent model is the continuous, maximum likelihood (Phillips *et al.*, 2004) of the occurrence of *L. invasa* based on environmental conditions; *Eucalyptus* species distribution and climate. Secondly, besides creating a more nuanced interpretation than presence-absence predictions (Arnold *et al.*, 2014; Jinga and Ashley, 2019), the continuous nature of the Maxent's output allows for fine relative distinctions to be made between the levels of pest risk in different areas. Finally, the Maxent model's generative approach to pest risk modelling - as opposed to a discriminative one - is advantageous when presence data are limited (Elith *et al.*, 2011).

One main limitation of the Maxent model in this study is that it did not (and does not in other studies) simulate for example biological control agents which might be released in places of pest infestation. Biological agents use natural mechanisms such as parasitism to reduce the population and intensity of pests (Masson *et al.*, 2017). It would thus be expected that the presence or absence of a biological agent, *Selitrichodes neseri* in this case, would contribute to a measure of environmental conditions favourable for the *L. invasa*. A second improvement that could be made to pest modelling in Maxent could be to go beyond depending on presence only

data by including aspects such as land cover and land uses in and around infested sites to improve predictability in the absence of pest presence data. A final limitation that affects the accuracy of presence only modelling relates to biases in the occurrence localities. In pest risk models, biases can occur depending on the pest dataset used. Using high resolution remotely sensed datasets rather than field-based observations can ameliorate location bias by providing a completer and more continuous dataset available for the study area and reducing sampling bias (Arnold *et al.*, 2014). However, it is important to acknowledge that biases and other uncertainties come with the use of remotely sensed data. Improvements in Maxent could be made to include more environmental predictor variables and intended human intervention to simulate possibilities and associated costs.

The Maxent presence-only model coupled with accurate projected climate data and r3PG have the potential to mitigate these losses by increasing the preparedness of forest managers. Unfortunately, the Maxent model remains largely qualitative. The extension of Maxent to quantify contextual potential yield loss could benefit from more detailed seasonal, multi-temporal and multi-spatial experiments that investigate; 1) the presence and intensity (on a scale) of *L. invasa* in a forest compartment; 2) the changes in the shape of sample leaves and the canopies of affected trees; 3) volume yield or mean annual increment (MAI) at each time of measurement. These data would theoretically be supported by climate data as was used in this study. Having a database with such variables would take the Maxent modelling beyond its current functionality. This is where integrating risk and process-based growth models into quantitative, economic-based models could quantify anticipated losses as well as required silvicultural interventions to contain the risk of pest infestations.

Further, the availability of quantifiable information on scheduled future management strategies like thinning and harvesting regimes could greatly improve the accuracy of predicting stand yield in forest plantations.

## 6 Conclusion

All other things staying constant, the *E. g x u* yield in the coastal Zululand region will be determined by reducing MAP (with increasing variability), increasing MAT, and increasing atmospheric CO<sub>2</sub>. Otherwise, more management interventions will be needed, as irrigation is infeasible for this resource. *E. g x u* is projected to perform better than *P. elliotii* in the region. It is recommended that similar tests and comparisons be made with other commercial tree species in South Africa.

That is why there is need to parameterise process-based models like 3PG for use on more species in more regions in South Africa.

An important possibility, worthy of deeper consideration, is that risk of *Leptocybe invasa* may well reduce in coastal Zululand, should its preferred bioclimatic variables conform to the projected climate trend. Combining future climate projections, process-based growth models like 3PG and pest risk models like Maxent with economic quantity-based models may provide useful information to improve the preparedness of forest managers and policy decision-making for the adaptation of the South African forestry industry to climate change. However, to improve the accuracy of predictions and models there is need now more than ever to develop more localised high-resolution climate data for the region as GCMs are still coarse in resolution.



## References

- ABARES (2011) *Potential effects of climate change on forests and forestry in Australia*. Canberra. Available at: [https://www.awe.gov.au/sites/default/files/documents/PotleffectsofClimateChngeOnForestandForestry\\_20110824\\_v1.0.0.pdf](https://www.awe.gov.au/sites/default/files/documents/PotleffectsofClimateChngeOnForestandForestry_20110824_v1.0.0.pdf).
- Abraha, M.G. and Savage, M.J. (2006) 'Potential impacts of climate change on the grain yield of maize for the midlands of KwaZulu-Natal, South Africa', *Agriculture, Ecosystems & Environment*, 115(1), pp. 150–160. doi:<https://doi.org/10.1016/j.agee.2005.12.020>.
- Almeida, A.C. (2003) *Application of a process-based model for predicting and explaining growth in Eucalyptus Plantations*. The Australian National University.
- Almeida, A.C., Sands, P.J., Bruce, J., Siggins, A.W., Leriche, A., Battaglia, M. and Batista, T.R. (2009) 'Use of a spatial process-based model to quantify forest plantation productivity and water use efficiency under climate change scenarios', *18th World IMACS Congress and MODSIM 2009 - International Congress on Modelling and Simulation: Interfacing Modelling and Simulation with Mathematical and Computational Sciences, Proceedings*, (July), pp. 1816–1822.
- Appelhans, T., Mwangomo, E., Hardy, D.R., Hemp, A. and Nauss, T. (2015) 'Evaluating machine learning approaches for the interpolation of monthly air temperature at Mt. Kilimanjaro, Tanzania', *Spatial Statistics*, 14, pp. 91–113. doi:[10.1016/j.spasta.2015.05.008](https://doi.org/10.1016/j.spasta.2015.05.008).
- Arnold, J.D., Brewer, S.C. and Dennison, P.E. (2014) 'Modeling climate-fire connections within the great basin and upper Colorado River Basin, Western United States', *Fire Ecology*, 10(2), pp. 64–75. doi:[10.4996/fireecology.1002064](https://doi.org/10.4996/fireecology.1002064).
- Barredo, J.I., Strona, G., de Rigo, D., Caudullo, G., Stancanelli, G. and San-Miguel-Ayanz, J. (2015) 'Assessing the potential distribution of insect pests: Case studies on large pine weevil (*Hylobius abietis* L) and horse-chestnut leaf miner (*Cameraria ohridella*) under present and future climate conditions in European forests', *EPPO Bulletin*, 45(2), pp. 273–281. doi:[10.1111/epp.12208](https://doi.org/10.1111/epp.12208).
- Basson, M.S. (2011) 'Water development in South Africa', in *UN-Water International Conference Water in the green economy in practice: Towards Rio+20*. Zaragoza: UN-Water. Available at: [http://www.un.org/waterforlifedecade/green\\_economy\\_2011/pdf/session\\_1\\_economic\\_instruments\\_south\\_africa.pdf](http://www.un.org/waterforlifedecade/green_economy_2011/pdf/session_1_economic_instruments_south_africa.pdf).
- Belgiu, M. and Drăgu, L. (2016) 'Random forest in remote sensing: A review of applications and future directions', *ISPRS Journal of Photogrammetry and Remote Sensing*, 114, pp. 24–31. doi:[10.1016/j.isprsjprs.2016.01.011](https://doi.org/10.1016/j.isprsjprs.2016.01.011).
- Bond, W., du Toit, J. and Malherbe, J. (2020) 'Special Issue: Drought in South African savannas', *African Journal of Range and Forage Science*, 37(1), pp. iii–v. doi:[10.2989/10220119.2020.1739197](https://doi.org/10.2989/10220119.2020.1739197).
- Bordoni, M., Valentino, R., Meisina, C., Bittelli, M. and Chersich, S. (2018) 'A simplified approach to assess the soil saturation degree and stability of a representative slope affected by shallow landslides in oltrepò pavese (Italy)', *Geosciences (Switzerland)*, 8(12). doi:[10.3390/geosciences8120472](https://doi.org/10.3390/geosciences8120472).
- Borges, J.S., Neves, J.C.L., Lourenço, H.M., Barros, N.F. de and Dias, S.C.M. (2012) 'Parameterization of the 3-PG model for eucalypt in the Region of Cerrado in Minas Gerais State',

*Ciência Florestal*, 22(3), pp. 567–578. doi:10.5902/198050986623.

Braconnot, P., Harrison, S.P., Otto-Bliesner, B.L., Abe-Ouchi, A., Jungclaus, J. and Peterschmitt, J.-Y. (2011) 'WCRP Coupled Model Intercomparison Project - Phase 5', *CLIVAR Exchanges Newsletter*, 16(56), pp. 1–52.

Bréda, N. and Brunette, M. (2019) 'Are 40 years better than 55? An analysis of the reduction of forest rotation to cope with drought events in a Douglas fir stand', *Annals of Forest Science*, 76(2), p. 29. doi:10.1007/s13595-019-0813-3.

Burkhardt, H.E. and Tomé, M. (2012) *Modeling forest trees and stands*. Dordrecht: Springer Netherlands. doi:10.1007/978-90-481-3170-9.

Camarero, J.J., Gazol, A., Sangüesa-Barreda, G., Cantero, A., Sánchez-Salguero, R., Sánchez-Miranda, A., Granda, E., Serra-Maluquer, X. and Ibáñez, R. (2018) 'Forest growth responses to drought at short- and long-term scales in Spain: Squeezing the stress memory from tree rings', *Frontiers in Ecology and Evolution*, 6(FEB), pp. 1–11. doi:10.3389/fevo.2018.00009.

Campion, J.M., Esprey, L.J. and Scholes, M.C. (2005) 'Application of the 3-PG model to a Eucalyptus grandis stand subjected to varying levels of water and nutritional constraints in KwaZulu-Natal, South Africa', *The Southern African Forestry Journal*, 203(1), pp. 3–13. doi:10.2989/10295920509505213.

De Cauwer, V., Knox, N., Kobue-Lekalake, R., Lepetu, J.P., Ompelege, M., Naidoo, S., Nott, A., Parduhn, D., Sichone, P., Tshwenyane, S., Elizabeth, Y. and Revermann, R. (2018) 'Woodland resources and management in southern Africa', *Biodiversity & Ecology*, 6(April), pp. 296–308. doi:10.7809/b-e.00337.

Christensen, J.H., Kanikicharla, K.K., Aldrian, E., An, S. II, Albuquerque Cavalcanti, I.F., de Castro, M., Dong, W., Goswami, P., Hall, A., Kanyanga, J.K., Kitoh, A., Kossin, J., Lau, N.C., Renwick, J., Stephenson, D.B., Xie, S.P., Zhou, T., Abraham, L., Ambrizzi, T., *et al.* (2013) 'Climate phenomena and their relevance for future regional climate change', *Climate Change 2013 the Physical Science Basis: Working Group I Contribution to the Fifth Assessment Report of the Intergovernmental Panel on Climate Change*, 9781107057, pp. 1217–1308. doi:10.1017/CBO9781107415324.028.

Church, J.A. and Gregory, J.M. (2019) 'Sea level change', *Encyclopedia of Ocean Sciences*, pp. 493–499. doi:10.1016/B978-0-12-409548-9.10820-6.

Clarke, L., Edmonds, J., Jacoby, H., Pitcher, H., Reilly, J. and Richels, R. (2007) *Scenarios of Greenhouse Gas Emissions and Atmospheric Concentrations Sub-report 2.1A of Synthesis and Assessment Product 2.1 by the U.S. Climate Change Science Program and the Subcommittee on Global Change Research*. Washington DC. Available at: <https://tntcat.iiasa.ac.at/RcpDb/dsd?Action=htmlpage&page=compare>.

Collins, M., Knutti, R., Arblaster, J., Dufresne, J.-L., Fichet, T., Friedlingstein, P., Gao, X., Gutowski, W.J., Johns, T., Krinner, G., Shongwe, M., Tebaldi, C., Weaver, A.J. and Wehner, M. (2013) 'Long-term climate change: Projections, commitments and irreversibility', in Stocker, T.F., Qin, D., Plattner, G.-K., Tignor, M., Allen, S.K., Boschung, J., Nauels, A., Xia, Y., Bex, V., and Midgley, P.M. (eds) *Climate Change 2013 the Physical Science Basis: Working Group I Contribution to the Fifth Assessment Report of the Intergovernmental Panel on Climate Change*. Cambridge: Cambridge University Press, pp. 1029–1136. doi:10.1017/CBO9781107415324.024.

Crous, J., Burger, L. and Sale, G. (2013) 'Growth response at age 10 years of five Eucalyptus genotypes planted at three densities on a drought-prone site in KwaZulu-Natal, South Africa',

*Southern Forests*, pp. 189–198. doi:10.2989/20702620.2013.820442.

Davis-Reddy, C.L. and Vincent, K. (2017) *Climate Risk and Vulnerability: A Handbook for Southern Africa*. 2nd edn. Pretoria: CSIR. Available at: [https://www.csir.co.za/sites/default/files/Documents/SADC\\_Handbook\\_Second\\_Edition\\_full\\_report.pdf](https://www.csir.co.za/sites/default/files/Documents/SADC_Handbook_Second_Edition_full_report.pdf).

Demory, M.-E., Berthou, S., Sørland, S., Roberts, M., Beyerle, U., Seddon, J., Haarsma, R., Schär, C., Christensen, O., Fealy, R., Fernandez, J., Nikulin, G., Peano, D., Putrasahan, D., Roberts, C., Steger, C., Teichmann, C. and Vautard, R. (2020) 'Can high-resolution GCMs reach the level of information provided by 12–50 km CORDEX RCMs in terms of daily precipitation distribution?', *Geoscientific Model Development Discussions*, (March), pp. 1–33. doi:10.5194/gmd-2019-370.

Department of Environmental Affairs (2014) *Climate Change Adaptation: Perspectives for the Southern African Development Community (SADC)*. Available at: [https://www.environment.gov.za/sites/default/files/docs/ltasphase2report1\\_adaptation\\_sadc.pdf](https://www.environment.gov.za/sites/default/files/docs/ltasphase2report1_adaptation_sadc.pdf).

Dike, V.N., Shimizu, M.H., Diallo, M., Lin, Z., Nwofor, O.K. and Chineke, T.C. (2015) 'Modelling present and future African climate using CMIP5 scenarios in HadGEM2-ES', *International Journal of Climatology*, 35(8), pp. 1784–1799. doi:10.1002/joc.4084.

Dlamini, L.S., Little, K.M., Sivparsad, B. and Nadel, R. (2019) 'Quantifying the impact of foliar insects on two Eucalyptus hybrids in Zululand, northern KwaZulu-Natal, South Africa', *South African Journal of Plant and Soil*, 36(2), pp. 129–135. doi:10.1080/02571862.2018.1499146.

Dosio, A., Jones, R.G., Jack, C., Lennard, C., Nikulin, G. and Hewitson, B. (2019) 'What can we know about future precipitation in Africa? Robustness, significance and added value of projections from a large ensemble of regional climate models', *Climate Dynamics*, 53(9–10), pp. 5833–5858. doi:10.1007/s00382-019-04900-3.

Dosio, A. and Jürgen, H. (2016) 'Climate change projections for CORDEX - Africa with COSMO - CLM regional climate model and differences with the driving global climate models', *Climate Dynamics*, 46(5), pp. 1599–1625. doi:10.1007/s00382-015-2664-4.

Dovey, S.B., du Toit, B. and de Clercq, W. (2011) 'Nutrient fluxes in rainfall, throughfall and stemflow in Eucalyptus stands on the Zululand coastal plain, South Africa', *Southern Forests*, 73(3–4), pp. 193–206. doi:10.2989/20702620.2011.639506.

Dube, T., Mutanga, O., Abdel-Rahman, E.M., Ismail, R. and Slotow, R. (2015) 'Predicting Eucalyptus spp. stand volume in Zululand, South Africa: an analysis using a stochastic gradient boosting regression ensemble with multi-source data sets', *International Journal of Remote Sensing*, 36(14), pp. 3751–3772. doi:10.1080/01431161.2015.1070316.

Dye, P.J. (2001) 'Modelling growth and water use in four pinus patula stands with the 3-pg model', *Southern African Forestry Journal*, 191(1), pp. 53–63. doi:10.1080/20702620.2001.10434151.

Dye, P.J., Jacobs, S. and Drew, D. (2004) 'Verification of 3-PG growth and water-use predictions in twelve Eucalyptus plantation stands in Zululand, South Africa', *Forest Ecology and Management*, 193(1–2), pp. 197–218.

Elith, J., Phillips, S.J., Hastie, T., Dudík, M., Chee, Y.E. and Yates, C.J. (2011) 'A statistical explanation of MaxEnt for ecologists', *Diversity and Distributions*, 17(1), pp. 43–57. doi:10.1111/j.1472-4642.2010.00725.x.

Elli, E.F. (2020) *Eucalyptus simulation models: understanding and mitigating the impacts of climate...* University of Sao Paulo. doi:10.11606/T.11.2020.tde-13082020-180005.

Elli, E.F., Sentelhas, P.C. and Bender, F.D. (2020) 'Impacts and uncertainties of climate change projections on Eucalyptus plantations productivity across Brazil', *Forest Ecology and Management*, 474(May), p. 118365. doi:10.1016/j.foreco.2020.118365.

Engelbrecht, F. (2019) *Green Book - Detailed Projections of Future Climate Change over South Africa*. Pretoria. Available at: [https://s3-eu-west-1.amazonaws.com/csir-greenbook/resources/WS2\\_ClimateChange\\_Report\\_2019.pdf](https://s3-eu-west-1.amazonaws.com/csir-greenbook/resources/WS2_ClimateChange_Report_2019.pdf).

Engelbrecht, F., Adegoke, J., Bopape, M.J., Naidoo, M., Garland, R., Thatcher, M., McGregor, J., Katzfey, J., Werner, M., Ichoku, C. and Gatebe, C. (2015) 'Projections of rapidly rising surface temperatures over Africa under low mitigation', *Environmental Research Letters*, 10(8). doi:10.1088/1748-9326/10/8/085004.

Engelbrecht, F.A., Landman, W.A., Engelbrecht, C.J., Landman, S., Bopape, M.M., Roux, B., McGregor, J.L. and Thatcher, M. (2011) 'Multi-scale climate modelling over Southern Africa using a variable-resolution global model', *Water SA*, 37(5), pp. 647–658. doi:10.4314/wsa.v37i5.2.

Esprey, L.J. (2005) *Assessment of a process-based model to predict the growth and yield of Eucalyptus grandis plantations in South Africa*. University of KwaZulu-Natal, Durban. Available at:

[https://researchspace.ukzn.ac.za/bitstream/handle/10413/1485/Esprey\\_Luke\\_John\\_2005.pdf?squence=1&isAllowed=y](https://researchspace.ukzn.ac.za/bitstream/handle/10413/1485/Esprey_Luke_John_2005.pdf?squence=1&isAllowed=y).

Fick, S.E. and Hijmans, R.J. (2017) 'WorldClim 2: new 1-km spatial resolution climate surfaces for global land areas', *International Journal of Climatology*, 37(12), pp. 4302–4315. doi:10.1002/joc.5086.

Flato, G., Marotzke, J., Abiodun, B., Braconnot, P., Chou, S.C., Collins, W., Cox, P., Driouech, F., Emori, S., Eyring, V., Forest, C., Gleckler, P., Guilyardi, E., Jakob, C., Kattsov, V., Reason, C. and Rummukainen, M. (2013) 'Evaluation of climate models', in Stocker, T.F., Qin, D., Plattner, G.-K., Tignor, M., Allen, S.K., Boschung, J., Nauels, A., Xia, Y., Bex, V., and Midgley, P.M. (eds) *Climate Change 2013 the Physical Science Basis: Working Group I Contribution to the Fifth Assessment Report of the Intergovernmental Panel on Climate Change*. Cambridge: Cambridge University Press, pp. 741–866. doi:10.1017/CBO9781107415324.020.

Gakenou, O.F. (2021) *Parameter testing and application of the 3PG model for Eucalyptus grandis x urophylla on the Zululand coastal plain, South Africa*. Stellenbosch University.

Germishuizen, I. and Mzinyane, T. (2017) 'Commercial forestry', in Mambo, J. and Faccor, K. (eds) *Understanding the Social & Environmental Implications of Global Change South African Risk and Vulnerability Atlas*. Second. Pretoria: AFRICAN SUN MeDIA, pp. 75–82. doi:10.1007/978-3-540-76435-9\_2137.

Giorgi, F. (2019) 'Thirty Years of Regional Climate Modeling: Where Are We and Where Are We Going next?', *Journal of Geophysical Research: Atmospheres*, 124(11), pp. 5696–5723. doi:10.1029/2018JD030094.

Girardin, M.P., Bernier, P.Y., Raulier, F., Tardif, J.C., Conciatori, F. and Guo, X.J. (2011) 'Testing for a CO<sub>2</sub> fertilization effect on growth of Canadian boreal forests', *Journal of Geophysical Research: Biogeosciences*, 116(1), pp. 1–16. doi:10.1029/2010JG001287.

Goble, B.J. and Elst, R. Van Der (2012) 'Trends in coastal development and land cover change:

The case of KwaZulu-Natal, South Africa', *Western Indian Ocean Journal of Marine Science*, 11(2), pp. 193–204.

Gupta, R. and Sharma, L.K. (2019) 'The process-based forest growth model 3-PG for use in forest management: A review', *Ecological Modelling*, 397(January), pp. 55–73. doi:10.1016/j.ecolmodel.2019.01.007.

Hijmans, R.J., Phillips, S., Leathwick, J. and Elith, J. (2021) 'Dismo. A R Package for species distribution modelling'. CRAN. Available at: <https://cran.r-project.org/web/packages/dismo/index.html>.

IPCC (2014) *Climate Change 2014: Synthesis Report, Contribution of Working Groups I, II and III to the Fifth Assessment Report of the Intergovernmental Panel on Climate Change*. Geneva, Switzerland.

Jewitt, D., Goodman, P.S., Erasmus, B.F.N., O'Connor, T.G. and Witkowski, E.T.F. (2015) 'Systematic land cover change in KZN implications for biodiversity', *South African Journal of Science*, 111(9), pp. 1–9.

Jinga, P. and Ashley, M. V. (2019) 'Climate change threatens some miombo tree species of sub-Saharan Africa', *Flora: Morphology, Distribution, Functional Ecology of Plants*, 257(February), p. 151421. doi:10.1016/j.flora.2019.151421.

Kassier, H.W. (2005) 'Angle count sampling as an alternative inventory method. Unpublished document.', p. 41.

Kirtman, B., Power, S.B., Adedoyin, A.J., Boer, G.J., Bojariu, R., Camilloni, I., Doblas-Reyes, F., Fiore, A.M., Kimoto, M., Meehl, G., Prather, M., Sarr, A., Schär, C., Sutton, R., van Oldenborgh, G.J., Vecchi, G. and Wang, H.J. (2013) 'Near-term climate change: Projections and predictability', *Climate Change 2013 the Physical Science Basis: Working Group I Contribution to the Fifth Assessment Report of the Intergovernmental Panel on Climate Change*, 9781107057, pp. 953–1028. doi:10.1017/CBO9781107415324.023.

Landman, W.A., Engelbrecht, F., Hewitson, B., Malherbe, J. and van der Merwe, J. (2018) 'Towards bridging the gap between climate change projections and maize producers in South Africa', *Theoretical and Applied Climatology*, 132(3–4), pp. 1153–1163. doi:10.1007/s00704-017-2168-8.

Landsberg, J.J. and Sands, P. (2011) 'Physiological Ecology of Forest Production: Principles, Processes and Models', in James, R.E., James, M., and Monica, G.T. (eds) *Terrestrial Ecology Series*. First edit. Academic Press, Elsevier, p. 352. doi:10.1016/B978-0-12-374460-9.00016-0.

Landsberg, J.J. and Waring, R.H. (1997) 'A generalised model of forest productivity using simplified concepts of radiation-use efficiency, carbon balance and partitioning', *Forest Ecology and Management*, 95(3), pp. 209–228. doi:10.1016/S0378-1127(97)00026-1.

Liaw, A. and Wiener, M. (2002) 'Classification and Regression by randomForest', *R News*, 2(December), pp. 18–22. Available at: [http://www.cmar.csiro.au/e-print/open/mcgregor\\_2005a.pdf](http://www.cmar.csiro.au/e-print/open/mcgregor_2005a.pdf).

Lopez, F.B. and Barclay, G.F. (2017) 'Chapter 4 - Plant Anatomy and Physiology', in Badal, S. and Delgoda, R. (eds) *Pharmacognosy*. Boston: Academic Press, pp. 45–60. doi:<https://doi.org/10.1016/B978-0-12-802104-0.00004-4>.

Lu, H., Xu, J., Li, G. and Liu, W. (2020) 'Site classification of Eucalyptus urophylla × Eucalyptus grandis plantations in China', *Forests*. doi:10.3390/f11080871.



- Lupo, A. and Kininmonth, W. (2013) *Global Climate Models and Their Limitations, Climate Change Reconsidered II: Physical Science*. Chicago. Available at: <http://climatechangereconsidered.org/wp-content/uploads/2019/01/CCR-II-Physical-Science-10-17-2013-entire-book.pdf>.
- Masson, M. V., Tavares, W.D.S., Lopes, F.D.A., Souza, A.R.D., Ferreira-Filho, P.J., Barbosa, L.R., Wilcken, C.F. and Zanuncio, J.C. (2017) 'Selitrichodes neseri (Hymenoptera: Eulophidae) Recovered from Leptocybe invasa (Hymenoptera: Eulophidae) Galls after Initial Release on Eucalyptus (Myrtaceae) in Brazil, and Data on Its Biology', *Florida Entomologist*, 100(3), pp. 589–593. doi:10.1653/024.100.0316.
- Maure, G., Pinto, I., Ndebele-Murisa, M., Muthige, M., Lennard, C., Nikulin, G., Dosio, A. and Meque, A. (2018) 'The southern African climate under 1.5 °c and 2 °c of global warming as simulated by CORDEX regional climate models', *Environmental Research Letters*, 13(6). doi:10.1088/1748-9326/aab190.
- Mcgregor, J.L. (2005) *C-CAM: Geometric Aspects and Dynamical Formulation*. Aspendale. Available at: [http://www.cmar.csiro.au/e-print/open/mcgregor\\_2005a.pdf](http://www.cmar.csiro.au/e-print/open/mcgregor_2005a.pdf).
- McSweeney, C.F., Jones, R.G., Lee, R.W. and Rowell, D.P. (2015) 'Selecting CMIP5 GCMs for downscaling over multiple regions', *Climate Dynamics*, 44(11–12), pp. 3237–3260. doi:10.1007/s00382-014-2418-8.
- Melesse, S.F. and Zewotir, T. (2017) 'Variation in growth potential between hybrid clones of Eucalyptus trees in eastern South Africa', *Journal of Forestry Research*, 28(6), pp. 1157–1167. doi:10.1007/s11676-017-0400-0.
- Mendel, Z., Protasov, A., Fisher, N. and La Salle, J. (2004) 'Taxonomy and biology of Leptocybe invasa gen. & sp. n. (Hymenoptera: Eulophidae), an invasive gall inducer on Eucalyptus', *Australian Journal of Entomology*, 43(2), pp. 101–113. doi:10.1111/j.1440-6055.2003.00393.x.
- De Micco, V., Carrer, M., Rathgeber, C.B.K., Julio Camarero, J., Voltas, J., Cherubini, P. and Battipaglia, G. (2019) 'From xylogenesis to tree rings: Wood traits to investigate tree response to environmental changes', *IAWA Journal*, 40(2), pp. 155–182. doi:10.1163/22941932-40190246.
- Mphahlele, M.M., Isik, F., Hodge, G.R. and Myburg, A.A. (2021) 'Genomic Breeding for Diameter Growth and Tolerance to Leptocybe Gall Wasp and Botryosphaeria/Teratosphaeria Fungal Disease Complex in Eucalyptus grandis', *Frontiers in Plant Science*, 12(February), pp. 1–15. doi:10.3389/fpls.2021.638969.
- Mrad, A., Manzoni, S., Oren, R., Vico, G., Lindh, M. and Katul, G. (2020) 'Recovering the Metabolic, Self-Thinning, and Constant Final Yield Rules in Mono-Specific Stands', *Frontiers in Forests and Global Change*, p. 62. Available at: <https://www.frontiersin.org/article/10.3389/ffgc.2020.00062>.
- Naidoo, S., Davis, C. and van Garderen, A. (2013) *Forests, rangelands and climate change in southern Africa*. 12. Rome.
- Naidoo, S., Davis, C. and Van Garderen, A. (2013) *Forests, rangelands and climate change in southern Africa*. 12. Rome.
- Najafi, R. and Hessami Kermani, M.R. (2017) 'Uncertainty Modeling of Statistical Downscaling to Assess Climate Change Impacts on Temperature and Precipitation', *Water Resources Management*, 31(6), pp. 1843–1858. doi:10.1007/s11269-017-1615-8.
- Nash, D.J., Klein, J., Endfield, G.H., Pribyl, K., Adamson, G.C.D. and Grab, S.W. (2019)

'Narratives of nineteenth century drought in southern Africa in different historical source types', *Climatic Change*, 152(3–4), pp. 467–485. doi:10.1007/s10584-018-2352-6.

Nash, D.J., Pribyl, K., Klein, J., Neukom, R., Endfield, G.H., Adamson, G.C.D. and Kniveton, D.R. (2016) 'Seasonal rainfall variability in southeast Africa during the nineteenth century reconstructed from documentary sources', *Climatic Change*, 134(4), pp. 605–619. doi:10.1007/s10584-015-1550-8.

Nguyen, T. Van, Mitlohner, R., Bich, N. Van and Do, T. Van (2015) 'Environmental Factors Affecting the Abundance and Presence of Tree Species in a Tropical Lowland Limestone and Non-limestone Forest in Ben En National Park, Vietnam', *Journal of Forest and Environmental Science*, 31(3), pp. 177–191. doi:10.7747/jfes.2015.31.3.177.

Nikulin, G., Asharaf, S., Magariño, M.E., Calmanti, S., Cardoso, R.M., Bhend, J., Fernández, J., Frías, M.D., Fröhlich, K., Früh, B., García, S.H., Manzanos, R., Gutiérrez, J.M., Hansson, U., Kolax, M., Liniger, M.A., Soares, P.M.M., Spirig, C., Tome, R., *et al.* (2018) 'Dynamical and statistical downscaling of a global seasonal hindcast in eastern Africa', *Climate Services*, 9(January 2017), pp. 72–85. doi:10.1016/j.cliser.2017.11.003.

Norby, R.J., Warren, J.M., Iversen, C.M., Childs, J., Jawdy, S.S. and Walker, A.P. (2021) 'Forest stand and canopy development unaltered by 12 years of CO<sub>2</sub> enrichment\*', *Tree Physiology*, pp. 1–13. doi:10.1093/treephys/tpab107.

Norby, R.J. and Zak, D.R. (2011) 'Ecological Lessons from Free-Air CO<sub>2</sub> Enrichment (FACE) Experiments', *Annual review of ecology, evolution, and systematics*, 42(1), pp. 181–203. doi:10.1146/annurev-ecolsys-102209-144647.

Nugnes, F., Gebiola, M., Monti, M.M., Gualtieri, L., Giorgini, M., Wang, J. and Bernardo, U. (2015) 'Genetic diversity of the invasive gall wasp *Leptocybe invasa* (Hymenoptera: Eulophidae) and of its *Rickettsia* endosymbiont, and associated sex-ratio differences', *PLoS ONE*. doi:10.1371/journal.pone.0124660.

Nxumalo, K.K.S. and Oladele, O.I. (2013) 'Factors Affecting Farmers' Participation in Agricultural Programme in Zululand District, Kwazulu Natal Province, South Africa', *Journal of Social Sciences*, 34(1), pp. 83–88. doi:10.1080/09718923.2013.11893120.

de Oliveira, R.A., Ramos, M.M. and de Aquino, L.A. (2015) 'Chapter 8 - Irrigation Management', in Santos, F., Borém, A., and Caldas, C. (eds) *Sugarcane*. San Diego: Academic Press, pp. 161–183. doi:https://doi.org/10.1016/B978-0-12-802239-9.00008-6.

Otieno, B.A., Nahrung, H.F. and Steinbauer, M.J. (2019) 'Where did you come from? Where did you go? Investigating the origin of invasive *Leptocybe* species using distribution modelling', *Forests*, 10(2). doi:10.3390/f10020115.

Peñuelas, J., Canadell, J.G. and Ogaya, R. (2011) 'Increased water-use efficiency during the 20th century did not translate into enhanced tree growth', *Global Ecology and Biogeography*, 20(4), pp. 597–608. doi:10.1111/j.1466-8238.2010.00608.x.

Pfeiffer, H.G. and Herman, A. (1943) 'the Origins of Beer ' S Law', (1), pp. 123–125.

Phillips, S.J., Anderson, R.P. and Schapire, R.E. (2005) 'Maximum entropy modeling of species geographic distributions', *Ecological Modelling*, 190(2006), pp. 231–259. doi:10.1016/j.ecolmodel.2005.03.026.

Phillips, S.J., Dudík, M. and Schapire, R.E. (2004) 'A maximum entropy approach to species distribution modeling', *Proceedings of the Twenty-First International Conference on Machine*



*Learning, ICML 2004*, pp. 655–662. doi:10.1145/1015330.1015412.

Pinto, I., Jack, C. and Hewitson, B. (2018) 'Process-based model evaluation and projections over southern Africa from Coordinated Regional Climate Downscaling Experiment and Coupled Model Intercomparison Project Phase 5 models', *International Journal of Climatology*, 38(11), pp. 4251–4261. doi:10.1002/joc.5666.

du Plessis, M. and Zwolinski, J. (2003) 'Site and stand analysis for growth prediction of eucalyptus grandis on the zululand coastal plain', *Southern African Forestry Journal*, 198(1), pp. 23–33. doi:10.1080/20702620.2003.10431732.

Power, S., Delage, F., Wang, G., Smith, I. and Kociuba, G. (2017) 'Apparent limitations in the ability of CMIP5 climate models to simulate recent multi-decadal change in surface temperature: implications for global temperature projections', *Climate Dynamics*, 49(1–2), pp. 53–69. doi:10.1007/s00382-016-3326-x.

R Core Team (2021) 'R: A language and environment for statistical computing.' Vienna, Austria.: R foundation for statistical computing.

Riahi, K., Gruebler, A. and Nakicenovic, N. (2007) 'Scenarios of long-term socio-economic and environmental development under climate stabilization', *Technological Forecasting and Social Change*, 7(74), pp. 887–935. Available at: <https://tntcat.iiasa.ac.at/RcpDb/dsd?Action=htmlpage&page=about>.

Sands, P. (2003) 'What is 3-PG?', *CRC for Sustainable Production Forestry and CSIRO Forestry and Forest Products*, 12.

Sands, P.J. (2010) '3PG PJS User Manual', (September), pp. 1–27.

Sands, P.J. and Landsberg, J.J. (2002) 'Parameterisation of 3-PG for plantation grown Eucalyptus globulus', *Forest Ecology and Management*, 163(1–3), pp. 273–292. doi:10.1016/S0378-1127(01)00586-2.

Saxton, K.E. and Rawls, W.J. (2006) 'Soil Water Characteristic Estimates by Texture and Organic Matter for Hydrologic Solutions', *Soil Science Society of America Journal*, 70(5), pp. 1569–1578. doi:10.2136/sssaj2005.0117.

Schulze, R.E. (2007) 'Soils: Agrohydrological Information Needs, Information Sources and Decision Support', in Schulze, R.E. (ed.) *South African Atlas of Climatology and Agrohydrology*. Pretoria, pp. 1–13.

Scolforo, H.F., de Castro Neto, F., Scolforo, J.R.S., Burkhart, H., McTague, J.P., Raimundo, M.R., Loos, R.A., da Fonseca, S. and Sartório, R.C. (2016) 'Modeling dominant height growth of eucalyptus plantations with parameters conditioned to climatic variations', *Forest ecology and management*, 380, pp. 182–195.

Scolforo, H.F., McTague, J.P., Burkhart, H., Roise, J., Alvares, C.A. and Stape, J.L. (2019) 'Modeling whole-stand survival in clonal eucalypt stands in Brazil as a function of water availability', *Forest Ecology and Management*, 432, pp. 1002–1012.

Scolforo, H.F., McTague, J.P., Burkhart, H., Roise, J., Campoe, O. and Stape, J.L. (2019) 'Eucalyptus growth and yield system: Linking individual-tree and stand-level growth models in clonal Eucalypt plantations in Brazil', *Forest Ecology and Management*, 432, pp. 1–16.

Seely, B., Welham, C. and Scoullar, K. (2015) 'Application of a hybrid forest growth model to evaluate climate change impacts on productivity, nutrient cycling and mortality in a montane forest

ecosystem', *PLoS ONE*, 10(8), pp. 1–25. doi:10.1371/journal.pone.0135034.

Sekulić, A., Kilibarda, M., Heuvelink, G.B.M., Nikolić, M. and Bajat, B. (2020) 'Random forest spatial interpolation', *Remote Sensing*, 12(10), pp. 1–29. doi:10.3390/RS12101687.

Sekulić, A., Kilibarda, M., Protić, D. and Bajat, B. (2021) 'A high-resolution daily gridded meteorological dataset for Serbia made by Random Forest Spatial Interpolation', *Scientific Data*, 8(1), pp. 1–12. doi:10.1038/s41597-021-00901-2.

Sibiya, G. (2021) *Predicting growth and future yield in Eucalyptus grandis x urophylla stands using the CABALA process-based model*. Stellenbosch University. Available at: <https://scholar.sun.ac.za/handle/10019.1/110324>.

Siderius, C., Gannon, K.E., Ndiyoi, M., Opere, A., Batisani, N., Olago, D., Pardoe, J. and Conway, D. (2018) 'Hydrological Response and Complex Impact Pathways of the 2015 / 2016 El Niño in Eastern and Southern Africa Earth ' s Future', *Earth's Future*, 6, pp. 2–22. doi:10.1002/ef2.268.

Simon, M.H., Ziegler, M., Bosmans, J., Barker, S., Reason, C.J.C. and Hall, I.R. (2015) 'Eastern South African hydroclimate over the past 270,000 years', *Scientific reports*, 5, p. 18153. doi:10.1038/srep18153.

Sithole, Z. (2011) *Parameterisation of the 3-PG process-based model in predicting the growth and water use of Pinus elliotii in South Africa*. University of KwaZulu-Natal.

Smith, C.W., Gardner, R.A.W., Pallett, R.N., Swain, T., Du Plessis, M. and Kunz, R.P. (2005) 'A site evaluation for site: species matching in the summer rainfall regions of southern Africa', *ICFR Bulletin*, (04), pp. 1–19.

Smith, S.J. and Wigley, T.M.L. (2006) 'Multi-Gas Forcing Stabilization with the MiniCAM', *Energy Journal*, (Special Issue #3), pp. 373–391. Available at: <https://tntcat.iiasa.ac.at/RcpDb/dsd?Action=htmlpage&page=about>.

Stape, J.L., Ryan, M.G. and Binkley, D. (2004) 'Testing the utility of the 3-PG model for growth of Eucalyptus grandis x urophylla with natural and manipulated supplies of water and nutrients', *Forest Ecology and Management*, 193(1–2), pp. 219–234. doi:10.1016/j.foreco.2004.01.031.

Subramanian, N., Nilsson, U., Mossberg, M. and Bergh, J. (2019) 'Impacts of climate Change, Weather Extremes and Alternative Strategies in Managed Forests', *Ecoscience*, 26(1), pp. 53–70. doi:10.1080/11956860.2018.1515597.

Tadross, M., Engelbrecht, F.A., Jack, C., Wolski, P. and Davis, C.L. (2017) 'Projected climate change futures for Southern Africa', in Davis-Reddy, C.L. and Vincent, K. (eds) *Climate risk and vulnerability A handbook for southern Africa*. Second. Pretoria: CSIR, pp. 20–29. Available at: <http://researchspace.csir.co.za/dspace/handle/10204/10101>.

Tang, J., Niu, X., Wang, S., Gao, H., Wang, X. and Wu, J. (2016) 'Statistical downscaling and dynamical downscaling of regional climate in China: Present climate evaluations and future climate projections', *Journal of Geophysical Research: Atmosphere*, 175(4449), p. 238. doi:10.1038/175238c0.

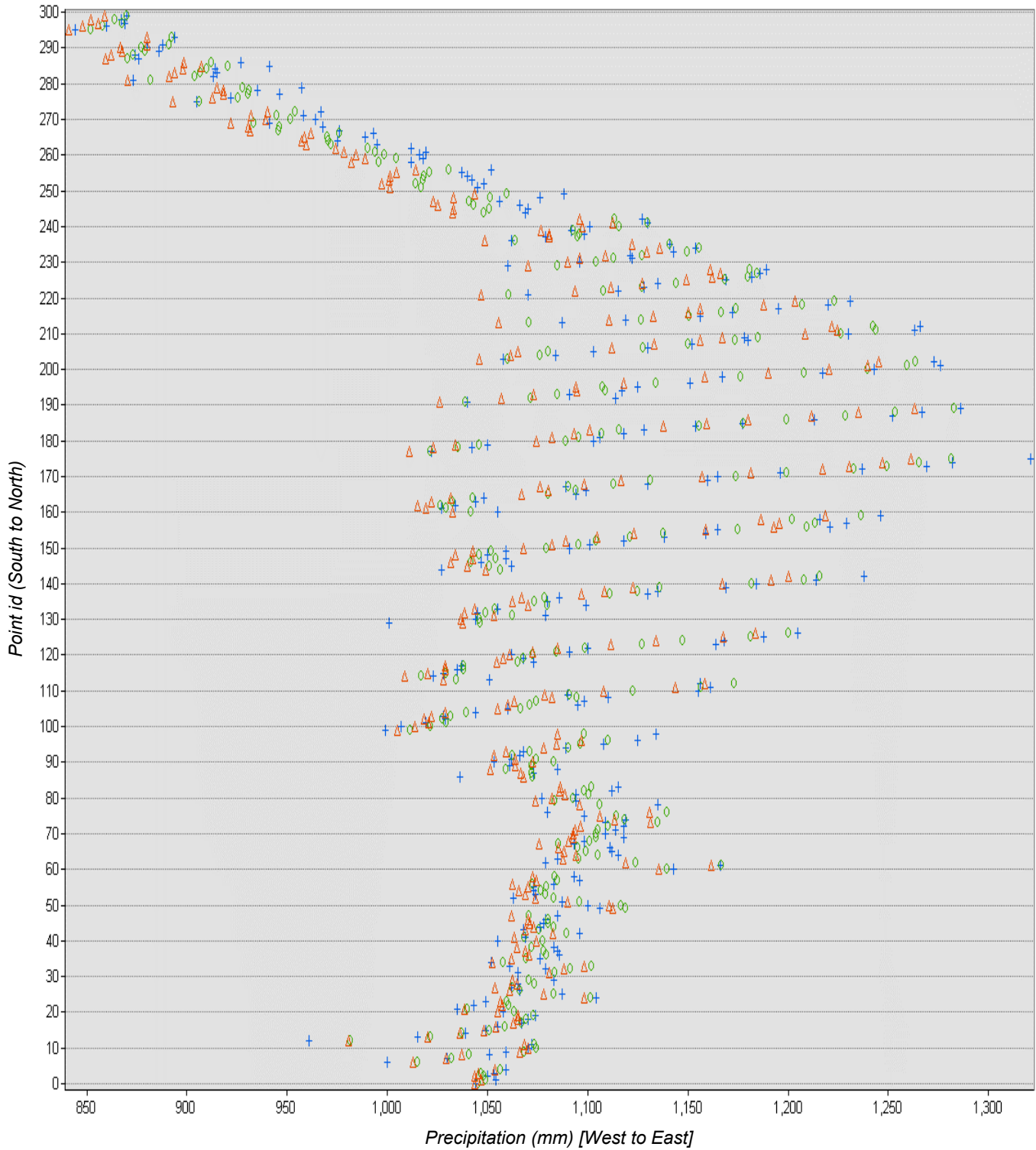
Taylor, K.E., Stouffer, R.J. and Meehl, G.A. (2012) 'An overview of CMIP5 and the experiment design', *Bulletin of the American Meteorological Society*, 93(4), pp. 485–498. doi:10.1175/BAMS-D-11-00094.1.

Tebaldi, C., Debeire, K., Eyring, V., Fischer, E., Fyfe, J., Friedlingstein, P., Knutti, R., Lowe, J., O'Neill, B., Sanderson, B., Van Vuuren, D., Riahi, K., Meinshausen, M., Nicholls, Z., Tokarska,

- K., Hurtt, G., Kriegler, E., Meehl, G., Moss, R., *et al.* (2021) 'Climate model projections from the Scenario Model Intercomparison Project (ScenarioMIP) of CMIP6', *Earth System Dynamics*, 12(1), pp. 253–293. doi:10.5194/esd-12-253-2021.
- Thompson, M., Gamage, D., Hirotsu, N., Martin, A. and Seneweera, S. (2017) 'Effects of elevated carbon dioxide on photosynthesis and carbon partitioning: A Perspective on root sugar sensing and hormonal crosstalk', *Frontiers in Physiology*, 8(AUG), pp. 1–13. doi:10.3389/fphys.2017.00578.
- Thomson, M.C., Abayomi, K., Barnston, A.G., Levy, M. and Dilley, M. (2003) 'El Niño and drought in southern Africa', *Lancet*, 361(9355), pp. 437–438. doi:10.1016/S0140-6736(03)12421-X.
- Trotsiuk, V., Hartig, F. and Forrester, D.I. (2020) 'r3PG – An R package for simulating forest growth using the 3-PG process-based model', *Methods in Ecology and Evolution*, 2020(August), pp. 1–6. doi:10.1111/2041-210x.13474.
- U.S. DOE (2020) *U.S. Department of Energy Free-Air CO<sub>2</sub> Enrichment Experiments: FACE Results, Lessons, and Legacy*. Oak Ridge. doi:10.2172/1615612.
- UNEP-DTU and CTCN (2017) *Downscaling of climate model projections*. Available at: <http://www.unepdhi.org/publications>.
- Walker, A.P., De Kauwe, M.G., Bastos, A., Belmecheri, S., Georgiou, K., Keeling, R.F., McMahon, S.M., Medlyn, B.E., Moore, D.J.P., Norby, R.J., Zaehle, S., Anderson-Teixeira, K.J., Battipaglia, G., Brienen, R.J.W., Cabugao, K.G., Cailleret, M., Campbell, E., Canadell, J.G., Ciais, P., *et al.* (2021) 'Integrating the evidence for a terrestrial carbon sink caused by increasing atmospheric CO<sub>2</sub>', *New Phytologist*, 229(5), pp. 2413–2445. doi:10.1111/nph.16866.
- Warburton, M. and Schulze, R. (2006) *Climate Change and the South African Commercial Forestry Sector: An Initial Study, ACRUcons Report 54*. Pietermaritzburg.
- Warburton, M.L. and Schulze, R.E. (2008) 'Potential impacts of climate change on the climatically suitable growth areas of Pinus and Eucalyptus: Results from a sensitivity study in South Africa', *Southern Forests*, 70(1), pp. 27–36. doi:10.2989/SOUTH.FOR.2008.70.1.5.515.
- Wise, M., Calvin, K., Thomson, A., Clarke, L., Bond-Lamberty, B., Sands, R., Smith, S., Janetos, A. and Edmonds, J. (2009) 'Implications of Limiting CO<sub>2</sub> Concentrations for Land Use and Energy', *Science*, 324, pp. 1183–1186.
- Wu, T., Lu, Y., Fang, Y., Xin, X., Li, L., Li, W., Jie, W., Zhang, J., Liu, Y., Zhang, L., Zhang, F., Zhang, Y., Wu, F., Li, J., Chu, M., Wang, Z., Shi, X., Liu, X., Wei, M., *et al.* (2019) 'The Beijing Climate Center Climate System Model (BCC-CSM): the main progress from CMIP5 to CMIP6', *Geoscientific Model Development*, 12(4), pp. 1573–1600. doi:10.5194/gmd-12-1573-2019.
- Xulu, S., Peerbhay, K., Gebreslasie, M. and Ismail, R. (2018) 'Drought influence on forest plantations in Zululand, South Africa, using MODIS time series and climate data', *Forests*, 9(9), pp. 1–15. doi:10.3390/f9090528.
- Xulu, S., Peerbhay, K., Gebreslasie, M. and Ismail, R. (2019) 'Unsupervised clustering of forest response to drought stress in Zululand region, South Africa', *Forests*, 10(7), pp. 1–15. doi:10.3390/f10070531.

# ANNEX 1 Mean annual precipitation change for each point in RCP 4.5

## Mean Annual Precipitation RCP 4.5



## ANNEX 2 Mean annual precipitation change for each point in RCP 4.5

### Mean Annual Precipitation RCP 8.5

